## Title
DR3 Regulates Intestinal Epithelial Homeostasis and Regeneration After Intestinal Barrier Injury



## Journal
Cellular and Molecular Gastroenterology and Hepatology, 16(1)

## ISSN
2352-345X

## Authors
Shimodaira, Yosuke
More, Shyam K
Hamade, Hussein
et al.

## Publication Date
2023

## DOI
10.1016/j.jcmgh.2023.03.008

Peer reviewed

cmgh
CELLULAR AND MOLECULAR GASTROENTEROLOGY AND HEPATOLOGY

ORIGINAL RESEARCH

# DR3 Regulates Intestinal Epithelial Homeostasis and Regeneration After Intestinal Barrier Injury

Yosuke Shimodaira,[1] Shyam K. More,[1] Hussein Hamade,[1] Anna Y. Blackwood,[1] Jay P. Abraham,[1] Lisa S. Thomas,[1] Jordan H. Miller,[1] Dalton T. Stamps,[1] Sofi L. Castanon,[1] Noam Jacob,[1,2,3] Connie W. Y. Ha,[1] Suzanne Devkota,[1] David Q. Shih,[1] Stephan R. Targan,[1] and Kathrin S. Michelsen[1,4]

*[1]F. Widjaja Foundation Inflammatory Bowel Disease Institute, Department of Medicine, Cedars-Sinai Medical Center, Los Angeles, California; [2]Vatche and Tamar Manoukian Division of Digestive Diseases, Department of Medicine, David Geffen School of Medicine, University of California Los Angeles, Los Angeles, California; [3]Division of Gastroenterology, Hepatology and Parenteral Nutrition, Veterans Affairs Greater Los Angeles Healthcare System, Los Angeles, CA; and [4]Department of Biomedical Sciences, Cedars-Sinai Medical Center, Los Angeles, California*

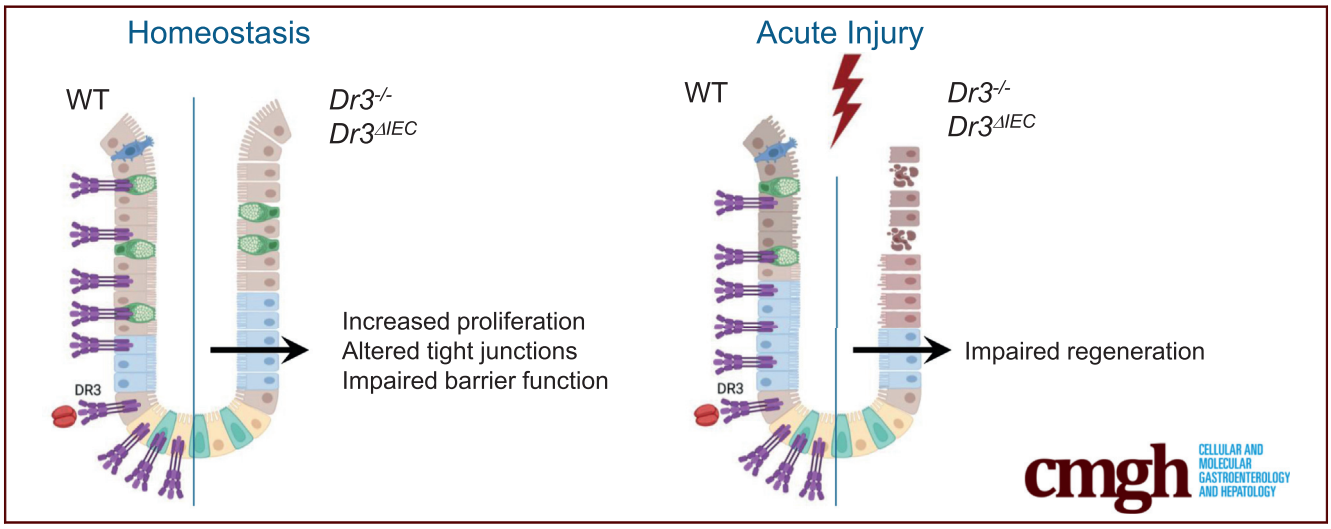


## SUMMARY

Expression of death receptor 3 in intestinal epithelial cells regulates intestinal permeability and cellular localization of tight junction proteins during homeostasis. As a result, *Dr3*$^{\Delta IEC}$ mice are more susceptible to acute colitis and show severely impaired epithelial barrier regeneration.

**BACKGROUND & AIMS:** Tumor necrosis factor (TNF) superfamily member tumor necrosis factor–like protein 1A (TL1A) has been associated with the susceptibility and severity of inflammatory bowel diseases. However, the function of the tumor necrosis factor–like protein 1A and its receptor death receptor 3 (DR3) in the development of intestinal inflammation is incompletely understood. We investigated the role of DR3 expressed by intestinal epithelial cells (IECs) during intestinal homeostasis, tissue injury, and regeneration.

**METHODS:** Clinical phenotype and histologic inflammation were assessed in C57BL/6 (wild-type), *Tl1a*$^{-/-}$ and *Dr3*$^{-/-}$ mice in dextran sulfate sodium (DSS)-induced colitis. We generated mice with an IEC-specific deletion of DR3 (*Dr3*$^{\Delta IEC}$) and assessed intestinal inflammation and epithelial barrier repair. In vivo intestinal permeability was assessed by fluorescein isothiocyanate dextran uptake. Proliferation of IECs was analyzed by bromodeoxyuridine incorporation. Expression of DR3 messenger RNA was assessed by fluorescent in situ hybridization. Small intestinal organoids were used to determine ex vivo regenerative potential.

**RESULTS:** *Dr3*$^{-/-}$ mice developed more severe colonic inflammation than wild-type mice in DSS-induced colitis with significantly impaired IEC regeneration. Homeostatic proliferation of IECs was increased in *Dr3*$^{-/-}$ mice, but blunted during regeneration. Cellular localization and expression of the tight junction proteins Claudin-1 and zonula occludens-1 were altered, leading to increased homeostatic intestinal permeability. *Dr3*$^{\Delta IEC}$ mice recapitulated the phenotype observed in *Dr3*$^{-/-}$ mice with increased intestinal permeability and IEC proliferation under homeostatic conditions and impaired tissue repair and increased bacterial translocation during DSS-induced colitis. Impaired regenerative potential and altered zonula occludens-1 localization also were observed in *Dr3*$^{\Delta IEC}$ enteroids.

**CONCLUSIONS:** Our findings establish a novel function of DR3 in IEC homeostasis and postinjury regeneration independent of

its established role in innate lymphoid cells and T-helper cells.
*(Cell Mol Gastroenterol Hepatol 2023;16:83–105; https://doi.org/10.1016/j.jcmgh.2023.03.008)*

*Keywords:* Intestinal Permeability; IEC Proliferation; Epithelial Barrier; Tissue Regeneration.

Intestinal homeostasis is tightly regulated by complex interactions between the intestinal mucosal immune network, intestinal epithelial cells (IECs), and intestinal microbiota.[1] Dysfunction in any of these mechanisms can lead to the development of intestinal inflammation and inflammatory bowel diseases (IBD). IBD results from integrated interactions between genetic susceptibility and severity genes that have an impact on the intestinal microbial environment and dysregulate innate and adaptive immune responses of the host against commensal microorganisms. IBD-associated single-nucleotide polymorphisms are enriched in genes that regulate epithelial barrier function, innate and adaptive immunity that could affect immune responses to commensal bacteria.[2]

Tumor necrosis factor (TNF)-like ligand 1A (TL1A), a TNF superfamily member originally described as a cytokine produced by endothelial and antigen-presenting cells, provides costimulatory signals to activated T cells and enhances their function via its receptor death receptor 3 (DR3).[3–5] Importantly, genetic polymorphisms in the genes *TNFSF15* encoding TL1A and *TNFRSF25* encoding DR3 have been associated with susceptibility to and severity of IBD.[6–10] Crohn's disease (CD) patients with *TNFSF15* risk haplotypes have increased expression of TL1A in intestinal mucosa and peripheral blood monocytes and are more prone to develop complications such as stricturing CD.[11–13] Mouse models that constitutively overexpress TL1A develop similar clinical phenotypes as human CD patients with risk variants. These mice develop spontaneous ileitis, intestinal fibrosis, and exacerbated dextran sulfate sodium (DSS)-induced chronic colitis.[11,14–16] However, mouse models of deficiencies of *Tl1a* or its receptor *Dr3*, as well as using neutralizing TL1A antibodies, have led to conflicting results. Although neutralizing TL1A antibodies prevent and reverse acute and chronic intestinal inflammation and reduce the development of intestinal fibrosis,[14,17,18] *Tl1a* or *Dr3* deficiency exacerbated acute DSS-induced colitis.[19,20] The role of TL1A and DR3 in these models has been attributed mainly to its function on different $T_{helper}$ ($T_H$) subsets, regulatory T cells, and innate lymphoid cells (ILCs).[17,19–21] In addition, it has been shown that DR3 is expressed on nonimmune cells, including IECs and fibroblasts, which could contribute to intestinal inflammation and fibrosis.[22,23] However, the exact mechanisms of how TL1A and DR3 affect intestinal inflammation, especially the role of DR3 expressed by IECs, and its contribution to the development of intestinal inflammation and tissue repair, still largely is unknown. This study aimed to investigate the role of TL1A–DR3 signaling on IECs and its contribution to intestinal inflammation.

IECs regulate the intestinal barrier function and protect against pathogenic and commensal luminal organisms. One of the mechanisms of IECs to maintain the physical barrier between luminal contents and the lamina propria is the expression of tight junction proteins, which regulate an impenetrable intact barrier. Dysregulated tight junction expression or intracellular localization elicits increased barrier permeability and susceptibility to DSS-induced murine colitis.[24–26] IEC proliferation, migration, and tight junction protein expression can be regulated by proinflammatory cytokines during inflammation. For example, TNF-$\alpha$, via its receptor Tumor necrosis factor receptor type II, affects a multitude of IEC functions including expression of tight junction proteins and maintenance of barrier function.[27–29] However, whether TL1A-DR3 signaling affects IEC function during homeostasis and inflammation still is unknown.

Here, we show that *Dr3* deficiency exacerbates acute and chronic DSS-induced colitis characterized by impaired intestinal epithelial regeneration, while *Tl1a*$^{-/-}$ mice developed a similar degree of colitis as wild-type (WT) mice. Under homeostatic conditions, we observed increased intestinal permeability, dysregulated expression of tight junction proteins, and uncontrolled IEC proliferation in *Dr3*$^{-/-}$ mice compared with WT mice. To elucidate the role of DR3 signaling in IECs, we generated mice with IEC-specific deletion of *Dr3* (*Dr3*$^{\Delta IEC}$). *Dr3*$^{\Delta IEC}$ mice recapitulate the phenotype of *Dr3*$^{-/-}$ mice under homeostatic conditions and during DSS-induced colitis. We observed increased intestinal permeability, altered tight junction protein expression, and increased IEC proliferation in *Dr3*$^{\Delta IEC}$ mice under homeostatic conditions. Strikingly, acute DSS colitis is exacerbated in *Dr3*$^{\Delta IEC}$ mice characterized by impaired intestinal epithelial regeneration, bacterial translocation to mesenteric lymph nodes (MLNs), and systemic inflammation. Consistent with these findings, we observed reduced regenerative potential of *Dr3*$^{\Delta IEC}$ ex vivo enteroid cultures and altered cellular localization of tight junction protein zonula occludens 1 (ZO-1). Our data establish a critical novel function of DR3 in regulating IEC homeostasis and uncover a mechanistic role of DR3 in IEC regeneration during mucosal injury.

## Results

### DR3 Deficiency Exacerbates DSS-Induced Chronic Colitis

First, we investigated the role of TL1A–DR3 signaling in a chronic model of colitis. Administration of 4 cycles of DSS

***Abbreviations used in this paper:*** **BrdU, bromodeoxyuridine; BSA, bovine serum albumin; CD, Crohn's disease; DPBS, Dulbecco's phosphate-buffered saline; DR3, death receptor 3; DSS, dextran sulfate sodium; FITC, fluorescein isothiocyanate; FoxP3, forkhead box P3; IBD, inflammatory bowel disease; IEC, intestinal epithelial cell; IFN-gamma, interferon gamma; IL, interleukin; ILC, innate lymphoid cell; ILC3, innate lymphoid cell type 3; LP, lamina propria; LPMC, lamina propria mononuclear cell; Mlck, myosin light-chain kinase; MLN, mesenteric lymph node; mRNA, messenger RNA; PBS, phosphate-buffered saline; RORγt, retinoid orphan receptor gamma t; SFB, segmented filamentous bacteria; sm-FISH, single-molecule fluorescent in situ hybridization; $T_H$, T helper; TL1A, tumor necrosis factor–like protein 1A; Treg, regulatory T cell; TUNEL, terminal deoxynucleotidyl transferase–mediated deoxyuridine triphosphate nick-end labeling; WT, wild-type; ZO-1, zonula occludens 1.**

**Most current article**


**2352-345X**
**https://doi.org/10.1016/j.jcmgh.2023.03.008**

in drinking water leads to the development of chronic colonic inflammation with characteristic $T_H1$ and $T_H17$ responses.[17] To investigate the specific roles of TL1A and DR3, we induced chronic DSS-induced colitis in TL1A-deficient (*Tl1a*$^{-/-}$), DR3-deficient (*Dr3*$^{-/-}$), and WT mice, and determined the clinical and pathologic characteristics of colitis. Interestingly, we observed bloody stool and severe diarrhea during each DSS cycle in *Dr3*$^{-/-}$ mice, while *Tl1a*$^{-/-}$ and WT mice had less severe symptoms (Figure 1*A*). Consistent with the stool phenotype, histologic scores as assessed by H&E staining showed that *Dr3*$^{-/-}$ mice developed more severe inflammation in the rectum and colon (Figure 1*B* and *C*). Interestingly, the significantly higher histologic score in *Dr3*$^{-/-}$ mice was driven mainly by a significantly higher regeneration subscore (score, 0–4, with 4 showing no tissue repair) compared with WT and *Tl1a*$^{-/-}$ mice, which is indicative of impaired epithelial regeneration in *Dr3*$^{-/-}$ mice (Figure 1*C* and *D*). DR3 is known to be expressed primarily in $CD4^+$ T cells and TL1A engagement induces the activation of several $T_H$ subsets, including $T_H1$, $T_H17$, $T_H9$, and regulatory T cells (Tregs).[17,30–34] However, we did not observe a significant difference in cell numbers or expression of the cytokines interferon gamma (IFN-gamma), interleukin (IL)17A, IL22, or IL10 between groups (Figure 2). We observed that forkhead box P3 ($FoxP3^+$) Tregs were reduced significantly in MLNs of *Dr3*$^{-/-}$ mice but not in the lamina propria (LP), as has been reported previously in acute DSS-induced colitis (Figure 2*C*).[20] Taken together, *Dr3*$^{-/-}$ mice develop exacerbated DSS-induced chronic colitis while intestinal inflammation in *Tl1a*$^{-/-}$ mice is comparable with WT mice. However, the more severe colonic inflammation in *Dr3*$^{-/-}$ mice was not associated with significant differences in $CD4^+$ $T_H$ cell responses.

## DR3 Regulates the Proliferation of IECs and Intestinal Permeability

Based on our results showing that the severe colonic inflammation in DSS-induced chronic colitis in *Dr3*$^{-/-}$ mice correlated with impaired intestinal epithelial regeneration, we hypothesized that *Dr3*$^{-/-}$ mice have impaired IEC function. To test for impaired epithelial barrier function, we first determined intestinal permeability for these mice during DSS colitis. *Dr3*$^{-/-}$ mice showed significantly higher fluorescein isothiocyanate (FITC) dextran permeability compared with WT mice (Figure 3*A*). To test whether the intestinal barrier is impaired in *Dr3*$^{-/-}$ mice under homeostatic conditions, we next performed intestinal permeability assays in 8-week-old untreated mice that did not show any signs of spontaneous intestinal inflammation. We observed that *Dr3*$^{-/-}$ mice have significantly increased permeability even under homeostatic uninflamed conditions (Figure 3*B*). Next, we investigated whether DR3 is involved in the maintenance of IECs. First, we assessed the expression of DR3 in IECs. A previous publication showed expression of DR3 in epithelial cell lines.[22] However, antibody-based detection of DR3 has been difficult in the past because of a lack of specificity of available anti-DR3 antibodies and we were unable to specifically detect DR3 with commercially available antibodies by immunofluorescence. Therefore, we performed single-molecule fluorescent in situ hybridization (sm-FISH) using a custom-made specific probe for murine *Dr3* messenger RNA (mRNA) and observed expression of DR3 in ileal and colonic IECs that was not observed in *Dr3*$^{-/-}$ intestinal tissue (Figure 4*A* and *B*). Furthermore, *Dr3* mRNA also was expressed in IECs from noninflamed areas of surgical specimens collected from CD patients (Figure 4*C*). We compared the expression of *Dr3* mRNA in inflamed and noninflamed ileal tissue sections from CD patients and did not observe differences in DR3 expression in IECs. Major differences in DR3 expression between inflamed and noninflamed tissue were observed in the LP, most likely as a result of infiltration of immune cells (Figure 4*D*). Furthermore, we analyzed the expression of *Dr3* mRNA in colonic tissue sections from a patient with diverticulitis (Figure 4*E*). Next, we assessed the baseline phenotype of IECs in *Dr3*$^{-/-}$ mice. We observed significantly increased villi length in the ileum and crypt length in the colon of *Dr3*$^{-/-}$ mice compared with WT mice (Figure 4*F* and *G*). Next, we assessed the proliferation and migration of IECs in *Dr3*$^{-/-}$ mice after bromodeoxyuridine (BrdU) incorporation under homeostatic conditions. Under homeostatic conditions, proliferating cells can be visualized by BrdU incorporation in transit-amplifying zones 2.5 hours after BrdU injection. At baseline, *Dr3*$^{-/-}$ mice have significantly higher numbers of proliferating IECs compared with WT mice in the ileum and colon (Figure 4*H* and *I*). These data indicate that DR3 regulates the proliferation of IECs. To determine if the increase in homeostatic proliferation in *Dr3*$^{-/-}$ mice is microbiota-dependent, we treated *Dr3*$^{-/-}$ mice with broad-spectrum antibiotics and assessed BrdU incorporation. We did not observe any significant differences in the numbers of proliferating IECs in the ileum or colon of antibiotic-treated *Dr3*$^{-/-}$ mice (Figure 4*J*). To investigate molecular mechanisms leading to increased permeability in *Dr3*$^{-/-}$ mice, we next studied the expression of several tight junction proteins at baseline. Compared with WT and *Tl1a*$^{-/-}$, ZO-1 expression in *Dr3*$^{-/-}$ mice is less continuous at the apical side of IECs and we observed more pronounced expression of ZO-1 and claudin-1 in the cytoplasm and at the basal–lateral membrane in *Dr3*$^{-/-}$ IECs (Figure 5*A*). We did not observe differences in the localization of claudin-2 or occludin in *Dr3*$^{-/-}$ compared with WT IECs (Figure 5*A*). We observed significantly increased mRNA expression of *claudin-1*, *claudin-4*, and *myosin light-chain kinase* (*Mlck*), and increased protein expression for claudin-1 in *Dr3*$^{-/-}$ IECs, but no differences in the expression of other tight junction proteins (claudin-2, -3, and -15) (Figure 5*B* and *C*). These data indicate that DR3 but not TL1A deficiency affects the subcellular location of tight junction proteins and their expression level. Collectively, DR3 deficiency affects IEC homeostasis, altering the rate of proliferation and turnover and distribution of tight junction proteins throughout the small and large intestine, leading to increased intestinal permeability.

## DR3 Deficiency Leads to Impaired IEC Regeneration and Proliferation During Acute DSS Colitis

To further investigate the increased IEC proliferation in *Dr3*$^{-/-}$ mice, we used the acute DSS model to assess epithelial cell regeneration. During acute DSS colitis, *Dr3*$^{-/-}$ mice

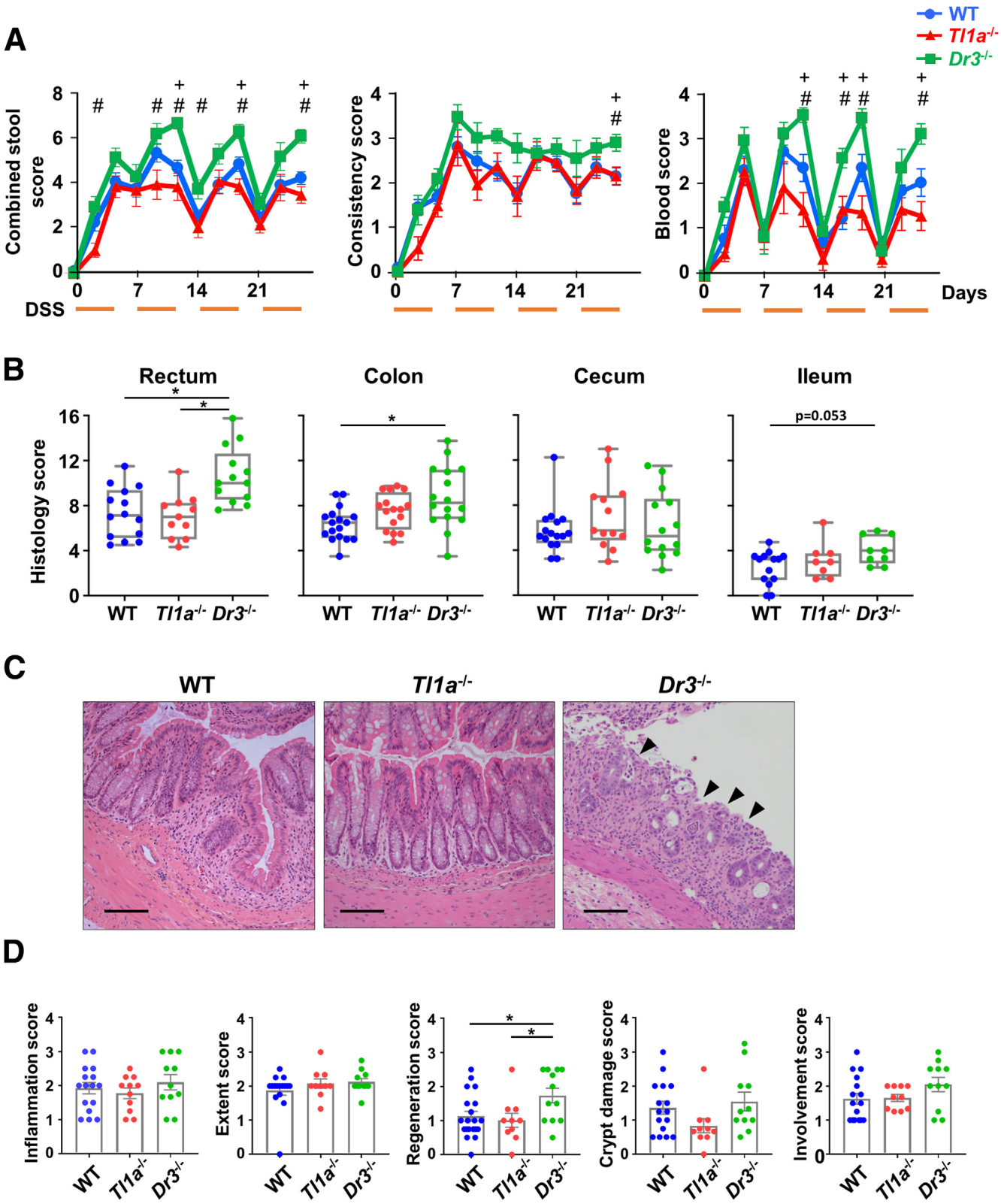


**Figure 1. DR3 deficiency exacerbates DSS-induced chronic colitis.** WT, *Tl1a*$^{-/-}$, and *Dr3*$^{-/-}$ mice underwent 4 cycles of 2.5% DSS to induce chronic colitis. (*A*) Combined stool scores (*left*; stool consistency plus blood in stool), consistency score (*middle*; 0, firm dry stool; 1, moist stool; 2, soft adherent stool; 3, large soft pliable stool; and 4, liquid stool), and blood score (*right*; 0, no color; 1, flecks of blue; 2, up to 50% blue; 3, >50% blue; and 4, gross red blood) during DSS-induced chronic colitis (N = 14–18/genotype). $^{+}P < .05$ for comparison between WT and *Dr3*$^{-/-}$, $^{\#}P < .05$ for comparison between *Tl1a*$^{-/-}$ and *Dr3*$^{-/-}$. (*B*) Histology scores. Data are presented as median with interquartile range. (*C*) Representative H&E staining of rectum. *Scale bar*: 100 $\mu$m. *Black arrowheads* indicate impaired regeneration of epithelial layer and ulcerations. (*D*) Histologic subscores for rectum. Each *dot* represents an individual mouse. Means ± SEM are shown. $^{*}P < .05$.

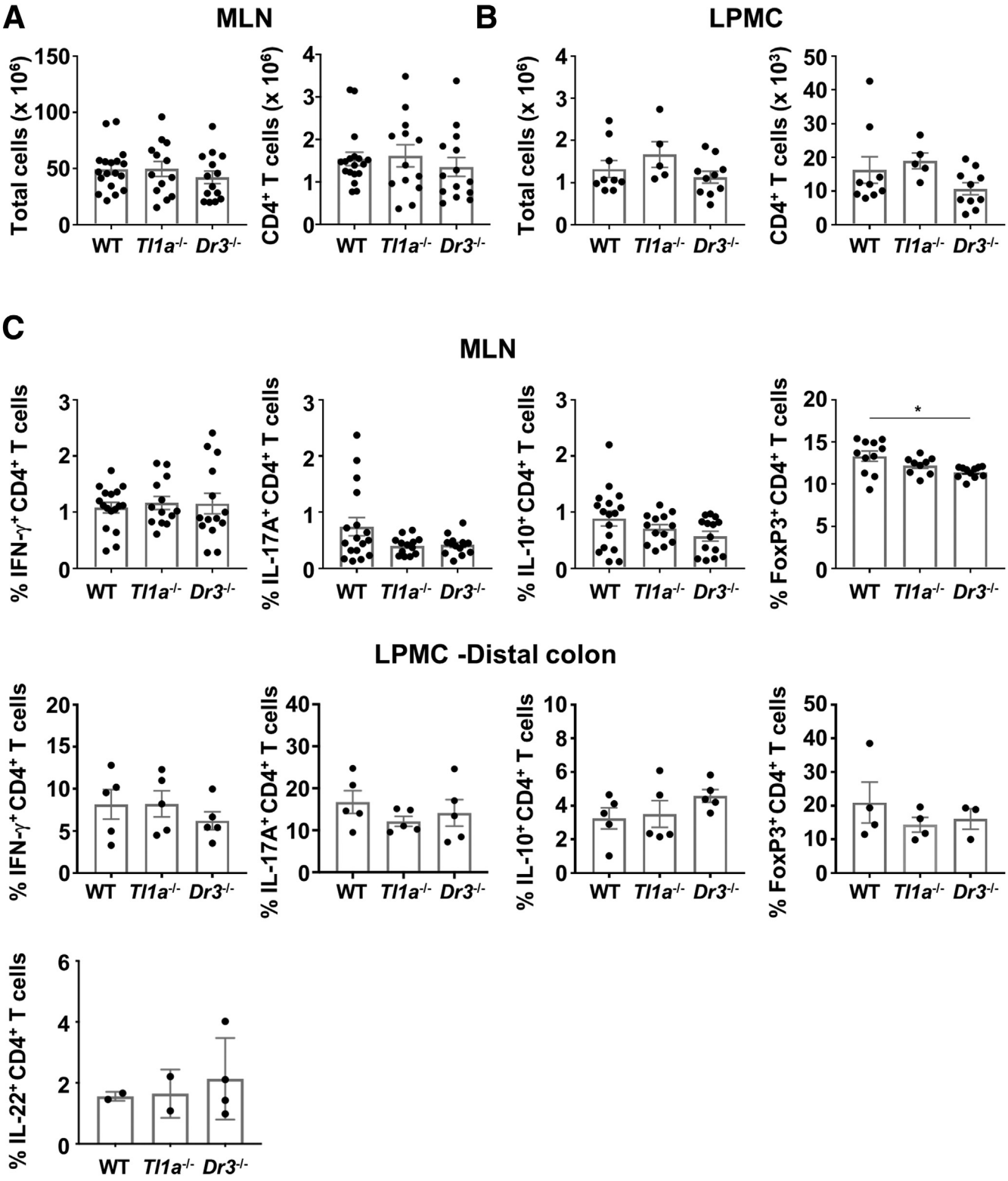


**Figure 2. $T_H1$, $T_H17$, and ILC3 responses are not altered in *Tl1a*$^{-/-}$ or *Dr3*$^{-/-}$ mice during chronic DSS colitis.** Cells were isolated from (*A*) MLNs and (*B*) LPMCs and the total number of cells and $CD4^+$ T cells was counted. (*B* and *C*) Isolated cells were incubated with phorbol 12-myristate 13-acetate and ionomycin for 4 hours. (*C*) Frequency of IFN-gamma, IL17A, IL10, IL22, and FoxP3-positive cells in MLNs (*top*) and LPMCs isolated from the distal colon (*bottom*) were assessed by intracellular staining using flow cytometry. Each *dot* represents an individual mouse. Means ± SEM are shown. $^*P < .05$.

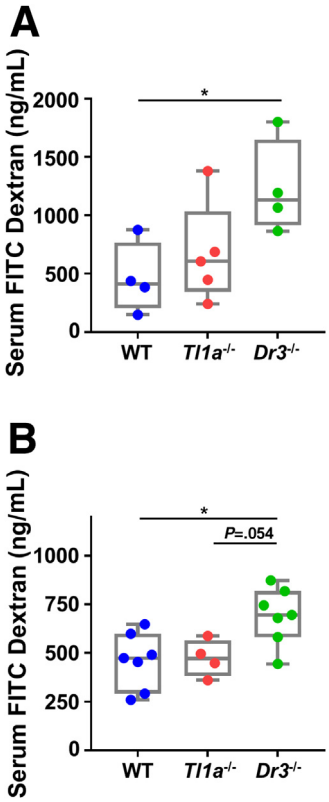


**Figure 3. DR3 deficiency increases intestinal permeability.** (*A*) WT, *Tl1a*$^{-/-}$, and *Dr3*$^{-/-}$ mice underwent 4 cycles of 2.5% DSS. On the day they were killed, mice were gavaged with FITC-dextran. The FITC-dextran serum concentration was measured 1 hour postgavage. (*B*) Untreated mice were gavaged with FITC-dextran. FITC-dextran serum concentrations are shown. Data are shown as median with interquartile range. Each *dot* represents an individual mouse. Data are from 3 independent experiments. *$P < .05$.

developed more severe intestinal inflammation compared with WT or *Tl1a*$^{-/-}$ mice, and had a higher stool score driven by a higher stool blood subscore (Figure 6*A*). Although microscopically injured tissue was covered by regenerating epithelial cells in WT mice, regeneration was strikingly impaired in *Dr3*$^{-/-}$ mice, which also was reflected by a significantly increased histology and regeneration score (Figure 6*B*). We also observed an increase in the size of spleens and significantly increased splenic cell numbers in *Dr3*$^{-/-}$ mice (Figure 6*C*), suggesting systemic inflammation caused by epithelial damage in these mice. In contrast, we did not observe any significant differences in LP total cell numbers, CD4$^{+}$ T-cell numbers, secretion of IFN-gamma, IL17A, or IL22 from lamina propria mononuclear cells (LPMCs), percentages of IL22$^{+}$ CD4$^{+}$ T cells, or IL22$^{+}$ retinoid orphan receptor gamma t (ROR$\gamma$t$^{+}$) innate lymphoid cell type 3 (ILC3s) in *Dr3*$^{-/-}$ compared with WT mice (Figure 6*D–G*). Interestingly, BrdU$^{+}$ cells were decreased in *Dr3*$^{-/-}$ compared with WT mice under inflammatory conditions (Figure 7*A* and *B*). Although WT mice responded to acute injury of the epithelial layer by significantly increased proliferation, in *Dr3*$^{-/-}$ mice the number of BrdU$^{+}$ cells was not increased over homeostatic proliferation, suggesting a blunted compensatory proliferation in response to injury in *Dr3*$^{-/-}$ mice (Figure 7*C*). These data indicate that while under homeostatic conditions DR3 deficiency leads to an increase in IEC proliferation, the regeneration of IECs is impaired in *Dr3*$^{-/-}$ mice after tissue injury. Next, we generated intestinal enteroids from the ileum of WT, *Tl1a*$^{-/-}$, and *Dr3*$^{-/-}$ mice to assess the functions of intestinal stem cells in ex vivo enteroid cultures. DR3 but not TL1A deficiency significantly reduced the enteroid surface area (Figure 8*A* and *B*). In contrast, the number of crypts was reduced significantly in *Tl1a*$^{-/-}$ and *Dr3*$^{-/-}$ enteroids (Figure 8*A* and *B*). Next, we analyzed ZO-1 expression by immunofluorescence staining in these enteroids. *Tl1a*$^{-/-}$ and *Dr3*$^{-/-}$ enteroids had significantly decreased ZO-1 fluorescence intensity compared with WT enteroids (Figure 8*C*). These results suggest compromised intestinal stem cell functions and expression of tight junction protein in *Dr3*$^{-/-}$ enteroids, while *Tl1a*$^{-/-}$ enteroid formation and surface area, indicative of proliferative response, is comparable with WT enteroids. However, *Tl1a*$^{-/-}$ enteroids have reduced de novo crypt formation, indicative of IEC differentiation, and ZO-1 expression compared with WT enteroids. Next, we analyzed mRNA expression of TL1A and DR3 in enteroids. Both TL1A and DR3 mRNA are expressed in WT enteroids (Figure 8*D*). To investigate direct effects of TL1A on enteroids, we first treated WT enteroids with TL1A. We observed significantly reduced enteroid surface area after TL1A treatment (Figure 8*E*). Next, we treated WT enteroids with a combination of TL1A and IL22. Although IL22 increased the enteroid surface area in a dose-dependent manner, as has been shown previously, addition of TL1A resulted in a similar increase in enteroid surface area compared with IL22 treatment alone (Figure 8*E*). These data suggest that IL22 treatment reverses the negative effects TL1A has on organoid formation. Finally, we treated enteroids derived from WT and *Dr3*$^{-/-}$ mice with IL22. We observed a significant increase in enteroid surface area and crypts per enteroid in both WT and *Dr3*$^{-/-}$ enteroids treated with IL22, suggesting that IL22 signaling is independent of DR3 signaling (Figure 8*F*).

## *Intestinal Epithelial DR3 Promotes the Integrity of the Intestinal Barrier and Regulated IEC Proliferation but Not Cell Death*

To address the functional importance of DR3 expressed on IECs we generated mice with DR3 deficiency in IECs by crossing Villin-Cre$^{+}$ with *Dr3*$^{fl/fl}$ mice (*Dr3*$^{\Delta IEC}$). We confirmed the cell-type–specific deletion of DR3 in *Dr3*$^{\Delta IEC}$ mice (Figure 9*A*). We observed significantly increased intestinal permeability in *Dr3*$^{\Delta IEC}$ compared with *Dr3*$^{fl/fl}$ mice under homeostatic conditions (Figure 9*B*). Furthermore, we also observed an increased serum IgA concentration in *Dr3*$^{\Delta IEC}$ mice while serum IgG concentrations were not significantly different between *Dr3*$^{\Delta IEC}$ and *Dr3*$^{fl/fl}$ mice, further corroborating an impaired intestinal barrier (Figure 9*C*). We did not observe any differences in fecal IgA concentrations between genotypes (Figure 9*C*). We

observed more pronounced expression of claudin-1 in the cytoplasm and at the basal–lateral membrane (Figure 9*D*), while apical claudin-1 expression in tight junctions was diminished. Overall, claudin-1 protein expression in *Dr3*$^{\Delta IEC}$ IECs was increased significantly (Figure 9*E*). IEC proliferation was increased significantly in *Dr3*$^{\Delta IEC}$ mice (Figure 9*F*

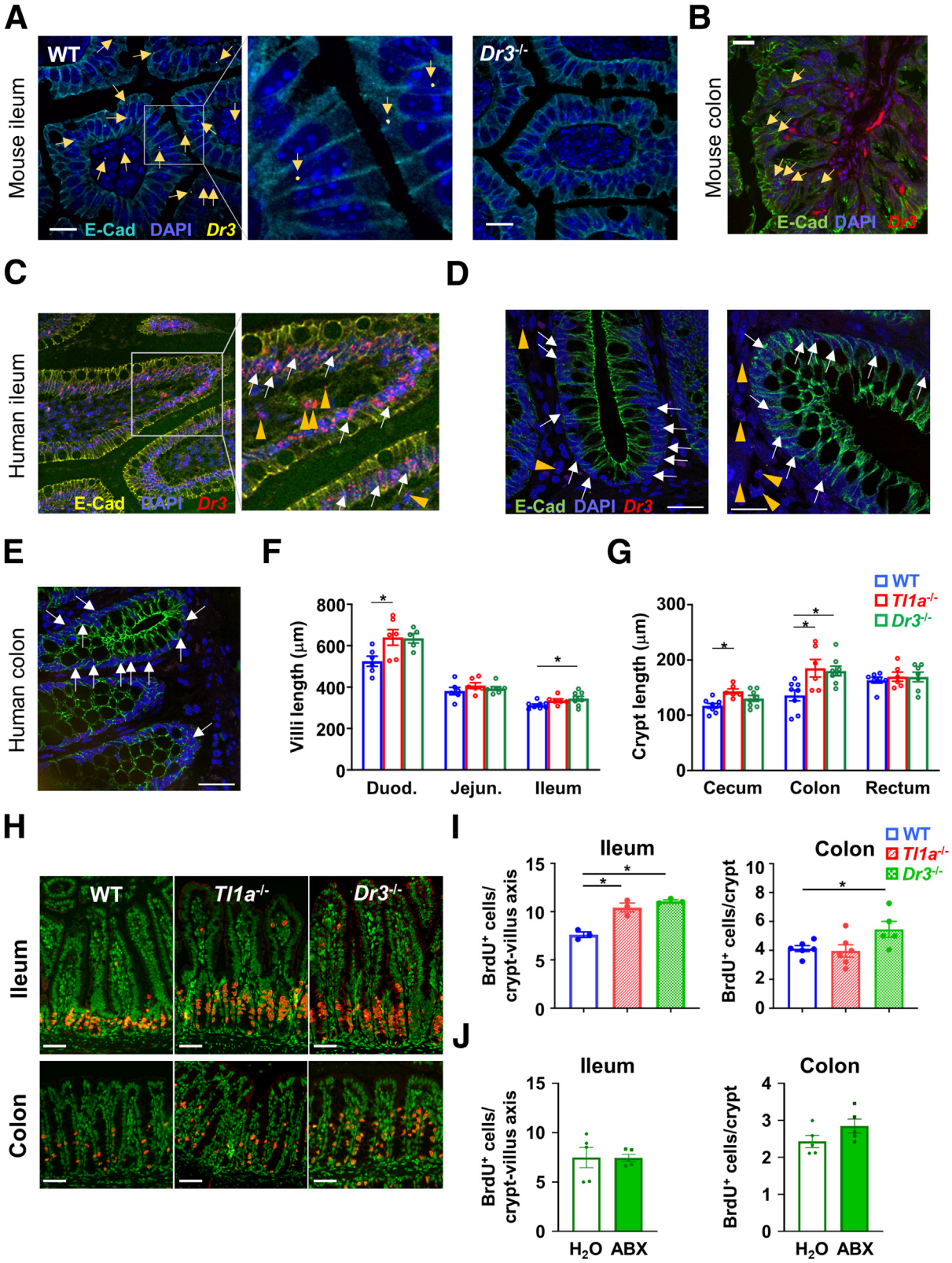

and *G*). DR3 signaling activates caspase 8 through the Fas Associated Via Death Domain pathway, which can induce apoptosis in certain cell types.[35,36] To determine the rate of homeostatic cell death, we performed terminal deoxynucleotidyl transferase–mediated deoxyuridine triphosphate nick-end labeling (TUNEL) staining, which detects apoptotic and necroptotic cell death. The number of TUNEL-positive cells was similar in ileal and colonic sections of *Dr3*$^{fl/fl}$ and *Dr3*$^{\Delta IEC}$ mice, indicating that cell death does not contribute to the compromised intestinal barrier in *Dr3*$^{\Delta IEC}$ mice (Figure 9*H*). These data indicate that DR3 expressed by IECs contributes directly to homeostatic proliferation and barrier function. Next, we determined if DR3 deficiency in IECs leads to differences in LP immune cell compositions. We did not observe any significant differences in LP total cell numbers; CD4$^+$ T-cell numbers; secretion of IFN-gamma, IL17A, or IL22 from LPMCs; percentages of IFN-gamma$^+$, IL17A$^+$, IL22$^+$, IL10$^+$ CD4$^+$ T cells; or IL22$^+$ ROR$\gamma$t$^+$ ILC3s under homeostatic conditions (Figure 10*A*–*D*). We also did not observe any significant difference in the relative abundance of segmented filamentous bacteria (SFB), a main inducer of IL22, between genotypes (Figure 10*E*). Similar to the results we obtained from *Dr3*$^{-/-}$ mice, we did not observe any significant differences in the number of proliferating IECs in the ileum or colon of antibiotic-treated *Dr3*$^{\Delta IEC}$ mice (Figure 10*F*).

## IEC-Specific Deletion of DR3 Leads to Growth Defects in Ileal Enteroids

The regenerative potential of intestinal stem cells was assessed by ileal ex vivo enteroid cultures. Enteroids prepared from *Dr3*$^{\Delta IEC}$ mice had significantly reduced surface area compared with *Dr3*$^{fl/fl}$ enteroids, indicating reduced proliferative potential (Figure 11*A* and *B*). The overall enteroid formation potential also was reduced in *Dr3*$^{\Delta IEC}$ enteroids (Figure 11*C*). We observed significantly reduced numbers of enteroids with 3 or more than 4 buds per enteroid in *Dr3*$^{\Delta IEC}$ compared with *Dr3*$^{fl/fl}$ enteroids (Figure 11*D*). Reduced surface area and impaired development of crypts in *Dr3*$^{\Delta IEC}$ enteroids suggest an impaired regenerative response. Staining of these enteroids with ZO-1 confirmed our findings of mislocalized tight junction proteins in *Dr3*$^{-/-}$ and *Dr3*$^{\Delta IEC}$ ileal tissues (Figures 5*A* and 7*E*). We observed discontinuous staining of ZO-1 in *Dr3*$^{\Delta IEC}$ enteroids, while ZO-1 staining was continuous and intact in *Dr3*$^{fl/fl}$ enteroids (Figure 11*E*).

## IEC-Specific Deletion of DR3 Exacerbates DSS-Induced Colitis and Impairs Proliferation and Regeneration

We next induced acute DSS-induced colitis in *Dr3*$^{\Delta IEC}$ mice. During acute colitis, we observed a more severe stool phenotype in *Dr3*$^{\Delta IEC}$ mice characterized by bloody diarrhea similar to the phenotype we observed in *Dr3*$^{-/-}$ mice (Figure 12*A*). We also observed more severe intestinal inflammation and a significantly higher histology score that was driven mainly by a significantly higher regeneration subscore, indicative of impaired IEC regeneration (Figure 12*B*). Consistent with our observations in *Dr3*$^{-/-}$ mice, we observed splenomegaly and an increased number of splenocytes in *Dr3*$^{\Delta IEC}$ mice (Figure 12*C*), suggesting systemic inflammation. Next, we assessed the degree of bacterial translocation from the LP to the draining lymph nodes by culturing MLN homogenates under anaerobic conditions. We observed a significant increase in the bacterial colonies in MLN homogenates from *Dr3*$^{\Delta IEC}$ mice compared with *Dr3*$^{fl/fl}$ mice (Figure 12*D*). Consistent with our data in *Dr3*$^{-/-}$ mice, the number of BrdU$^+$ cells was similar in *Dr3*$^{\Delta IEC}$ compared with *Dr3*$^{fl/fl}$ under inflammatory conditions (Figure 12*E* and *F*). Although *Dr3*$^{fl/fl}$ mice responded to acute injury by increased proliferation, in *Dr3*$^{\Delta IEC}$ mice the number of BrdU$^+$ cells was not increased over homeostatic proliferation, suggesting a blunted compensatory proliferation in response to injury in *Dr3*$^{\Delta IEC}$ mice (Figure 12*G*). Next, we determined the LP immune cell compositions after acute DSS injury in *Dr3*$^{fl/fl}$ and *Dr3*$^{\Delta IEC}$ mice. We did not observe any significant differences in LP total cell numbers; CD4$^+$ T-cell numbers; secretion of IFN-gamma, IL17A, or IL22 from LPMCs or ileal explants; percentages of IFN-gamma$^+$, IL17A$^+$, IL10$^+$ CD4$^+$ T cells; or IL22$^+$ ROR$\gamma$t$^+$ ILC3s after acute DSS injury (Figure 13). We did observe a significant increase in LP IL22$^+$ CD4$^+$ T cells in *Dr3*$^{\Delta IEC}$ mice (Figure 13*D*). Collectively, these results show a key role for DR3 signaling on IECs in regulating homeostatic IEC proliferation and barrier function and protecting from bacterial dissemination and promoting tissue repair after intestinal injury.

**Figure 4.** (***See previous page***). ***Dr3*$^{-/-}$ mice have increased homeostatic IEC proliferation.** (*A*) Ileal villi of WT (*left*) and *Dr3*$^{-/-}$ (*right*) mice were analyzed for *Dr3* expression by sm-FISH. *Dr3* (yellow), 4',6-diamidino-2-phenylindole (DAPI) (blue), and E-cadherin (cyan). *Arrows* indicate *Dr3*-expressing cells. *Scale bar*: 20 $\mu$m. (*B*) Colonic crypts of WT mice were analyzed for *Dr3* expression by sm-FISH. *Dr3* (red), DAPI (blue), and E-cadherin (green). *Arrows* indicate *Dr3*-expressing cells. (*C*–*E*) *Dr3* expression in human ileal and colonic tissue. (*C*) Healthy human ileal tissue. *Dr3* (red), DAPI (blue), and E-cadherin (yellow). (*D*) Noninflamed (*left*) and inflamed (*right*) ileal tissue from a CD patient. *White arrows* indicate *Dr3* expression in IECs and *yellow arrowheads* indicate *Dr3* expression in LP cells. *Scale bar*: 25 mm. (*E*) Colonic tissue from a patient with diverticulitis. *Dr3* (red), DAPI (blue), and E-cadherin (green). *White arrows* indicate *Dr3* expression in IECs. *Scale bar*: 25 $\mu$m. (*F*) Villi length of small intestine and (*G*) crypt length of large intestines are shown (N = 6–7 mice/genotype). (*H* and *I*) WT, *Tl1a*$^{-/-}$, and *Dr3*$^{-/-}$ mice were injected intraperitoneally with BrdU 2.5 hours before being killed. (*H*) Representative ileal and colonic BrdU staining (red) co-stained with DAPI (green). *Scale bar*: 50 $\mu$m. (*I*) Quantification of BrdU$^+$ cells in tissue sections. BrdU$^+$ cells were counted in 20 well-oriented crypt–villi axis. Each *dot* represents the average of BrdU$^+$ cells/crypt–villi axis of an individual mouse. (*J*) *Dr3*$^{-/-}$ mice were treated with or without broad-spectrum antibiotics for 4 weeks. Quantification of BrdU$^+$ cells in tissue sections. BrdU$^+$ cells were counted in 20 well-oriented crypt–villi axis. Each *dot* represents the average of BrdU$^+$ cells/crypt–villi axis of an individual mouse. Means ± SEM are shown. *$P < .05$. ABX, antibiotics; Duod, duodenum; E-cad, E-cadherin; Jejun, jejunum.

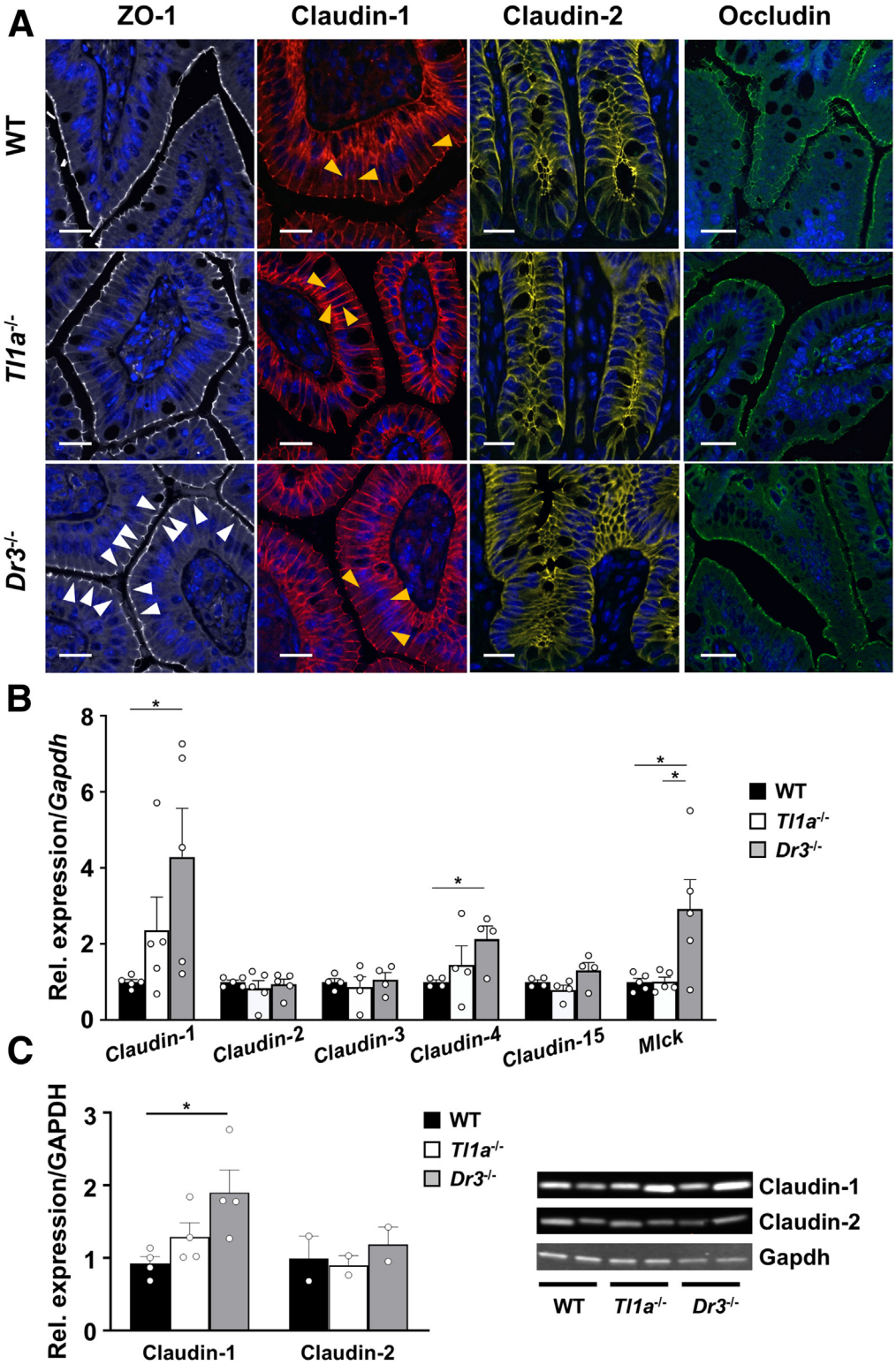


**Figure 5. DR3 regulates the expression and subcellular localization of tight junction proteins ZO-1 and claudin-1.** (*A*) Representative ileal images of immunofluorescence of ZO-1 (gray), claudin-1 (red), claudin-2 (yellow), occludin (green), and DAPI (blue) staining in WT (*top*), *Tl1a*$^{-/-}$ (*middle*), and *Dr3*$^{-/-}$ (*bottom*) mice. *White arrowheads* indicate discontinued ZO-1 staining at the apical side of the IEC layer. *Yellow arrowheads* indicate normal claudin-1 staining at tight junctions in WT and *Tl1a*$^{-/-}$ mice, but diminished claudin-1 staining at tight junctions in *Dr3*$^{-/-}$ mice. *Scale bar*: 20 $\mu$m. (*B*) Relative mRNA expression of *claudin-1*, *-2*, *-3*, *-4*, and *-15*, and *Mlck* in colonic epithelial cells was assessed by quantitative polymerase chain reaction (N = 5/genotype). (*C*) Protein expression in ileal epithelial cells was assessed by Western blot. Relative expression of claudin-1 and claudin-2 are shown (*left*; N = 4/genotype). Representative images of Western blots (*right*). Means ± SEM, $^*P < .05$, Student *t* test. GAPDH, glyceraldehyde-3-phosphate dehydrogenase; Rel, relative.

## Discussion

Our data highlight the role of the IBD-associated genes *TNFSF15* (TL1A) and its receptor *TNFRSF25* (DR3) as major regulators of intestinal epithelial barrier function. Previous publications that focused on the role of mucosal TL1A–DR3 signaling in innate and adaptive immune responses reported conflicting results, suggesting a complex, dual role of this pathway under homeostatic and inflammatory

conditions. Although neutralizing TL1A antibodies prevented and reversed acute and chronic intestinal inflammation,[14,17] *Tl1a* or *Dr3* deficiency exacerbated acute DSS-induced colitis.[19,20] Overexpression of TL1A in transgenic mice causes spontaneous ileitis and fibrosis, thereby mimicking the phenotype of CD patients with *TNFSF15* risk

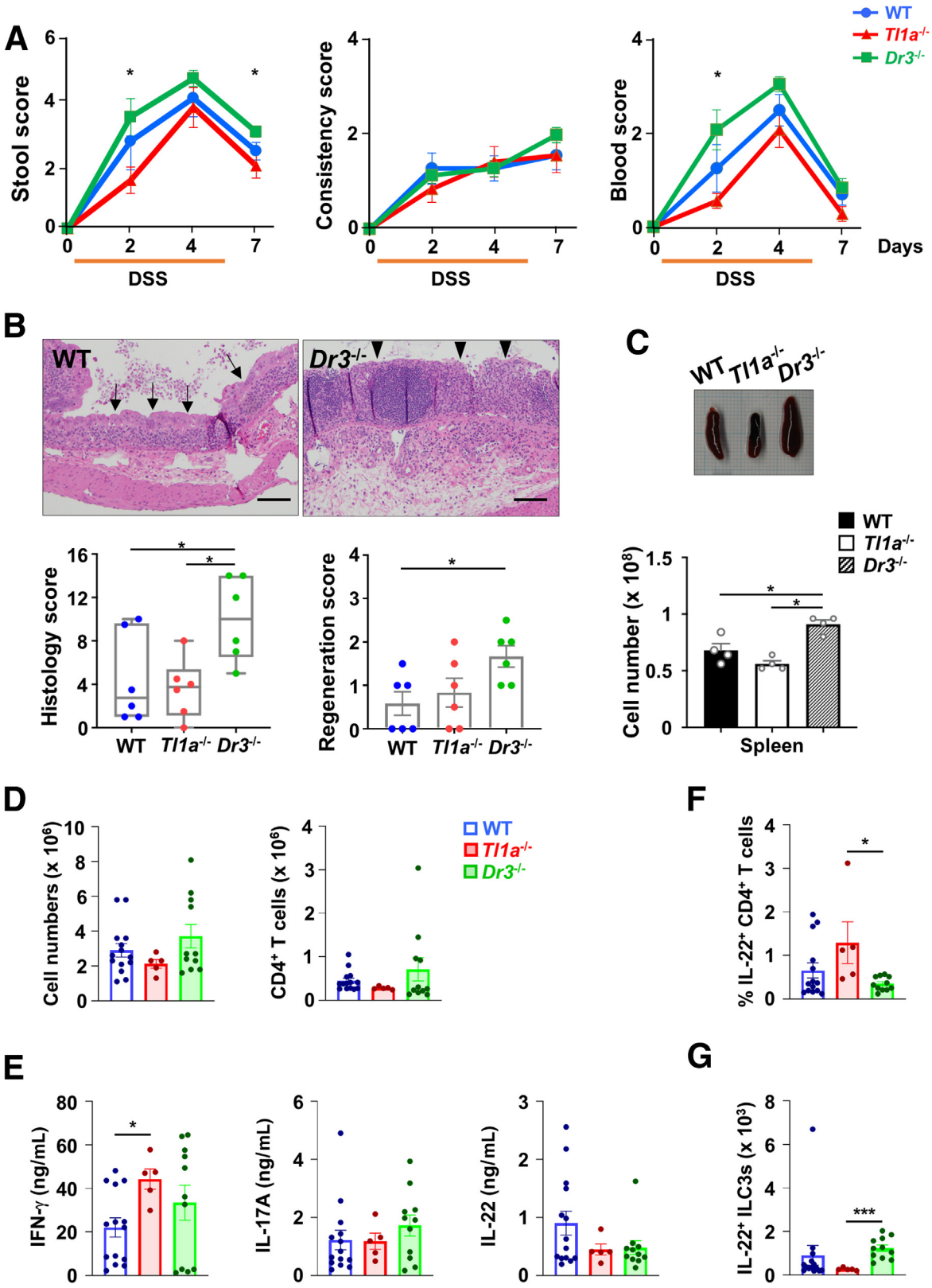

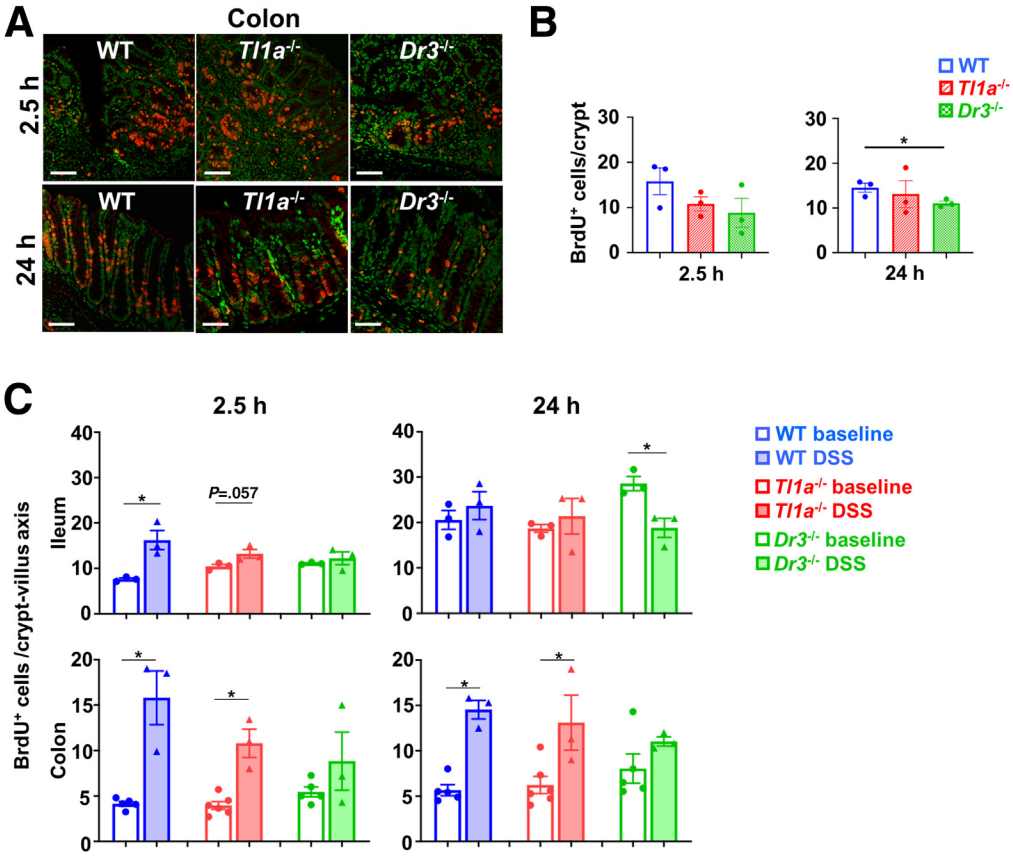


**Figure 7. DR3 deficiency impairs IEC proliferation in DSS-induced epithelial damage.** WT, *Tl1a*$^{-/-}$, and *Dr3*$^{-/-}$ mice were treated with 3% DSS for 5 days and regular drinking water for 2 days. Mice were injected intraperitoneally with BrdU 2.5 or 24 hours before being killed. (*A*) Representative colonic BrdU staining (red) co-stained with DAPI (green). *Scale bar*: 50 $\mu$m. (*B*) Quantification of BrdU$^+$ cells in colonic tissue sections. BrdU$^+$ cells were counted in 20 well-oriented crypts. Each *dot* represents the average BrdU$^+$ cells/crypt axis of an individual mouse. (*C*) Quantification of BrdU$^+$ cells in ileal (*top*) and colon (*bottom*) tissue sections. BrdU$^+$ cells were counted in 20 well-oriented crypts. Each symbol represents the average of BrdU$^+$ cells/crypt–villus axis of an individual mouse. Means ± SEM are shown. *$P < .05$.

polymorphisms.[11,14,18] The role of TL1A and DR3 in these models has been attributed mainly to its function on different $T_H$ subsets, regulatory T cells, and particularly ILCs.[17–20] In this study, we investigated the contribution of TL1A–DR3 signaling in epithelial cells to intestinal pathologies by generating cell type–specific genetic deletion of DR3 on IECs. Our results help to reconcile some of the conflicting results observed in these models by showing an important role for DR3 in intestinal epithelial barrier maintenance under homeostatic conditions and repair after injury. Although neutralizing anti-TL1A antibodies transiently lowers pathophysiological TL1A concentrations in mucosal tissues to physiological concentrations and thereby has therapeutic effects, a complete lack of either TL1A or DR3 has detrimental effects in DSS colitis.[17,19,20] It is plausible that a complete lack of TL1A or DR3 in *Tl1a*$^{-/-}$ or *Dr3*$^{-/-}$

**Figure 6.** (***See previous page***). **DR3 deficiency impairs tissue regeneration in DSS-induced epithelial damage.** WT, *Tl1a*$^{-/-}$, and *Dr3*$^{-/-}$ mice were treated with 3% DSS for 5 days and regeneration was analyzed 2 or 3 days after DSS treatment. (*A*) Combined stool scores (*left*), consistency score (*middle*), and blood score (*right*) at the indicated time points (N = 6/genotype). *$P < .05$ for comparison between *Tl1a*$^{-/-}$ and *Dr3*$^{-/-}$. (*B*) Representative H&E staining of WT and *Dr3*$^{-/-}$ rectal tissue (*top*), histology score (*bottom left*), and regeneration score (*bottom right*) are shown. *Black arrows* indicate regenerating epithelial layer, and *black arrowheads* indicate ulcerations. Each *dot* represents an individual mouse. *Scale bar*: 100 $\mu$m. (*C*) Representative macroscopic images of spleens (*top*) and splenocyte numbers (*bottom*) from 2 independent experiments. (N = 4/genotype). (*D–G*) WT, *Tl1a*$^{-/-}$, and *Dr3*$^{-/-}$ mice were treated with 3% DSS for 3 days to induce acute colitis. (*D*) Cells were isolated from LP and the total number of cells (*left*) and CD4$^+$ T cells (*right*) were counted. (*E*) Enzyme-linked immunosorbent assay analysis of IFN-gamma, IL17A, and IL22 production from LPMCs after ex vivo restimulation with anti-CD3 and anti-CD28. (*F*) Frequency of IL22-positive cells in LPMCs isolated from the large intestine were assessed by intracellular staining using flow cytometry. (*G*) Total numbers of IL22-positive ROR$\gamma$t$^+$ ILC3s in LPMCs isolated from the large intestine. Each *dot* represents an individual mouse. Means ± SEM are shown. *$P < .05$.

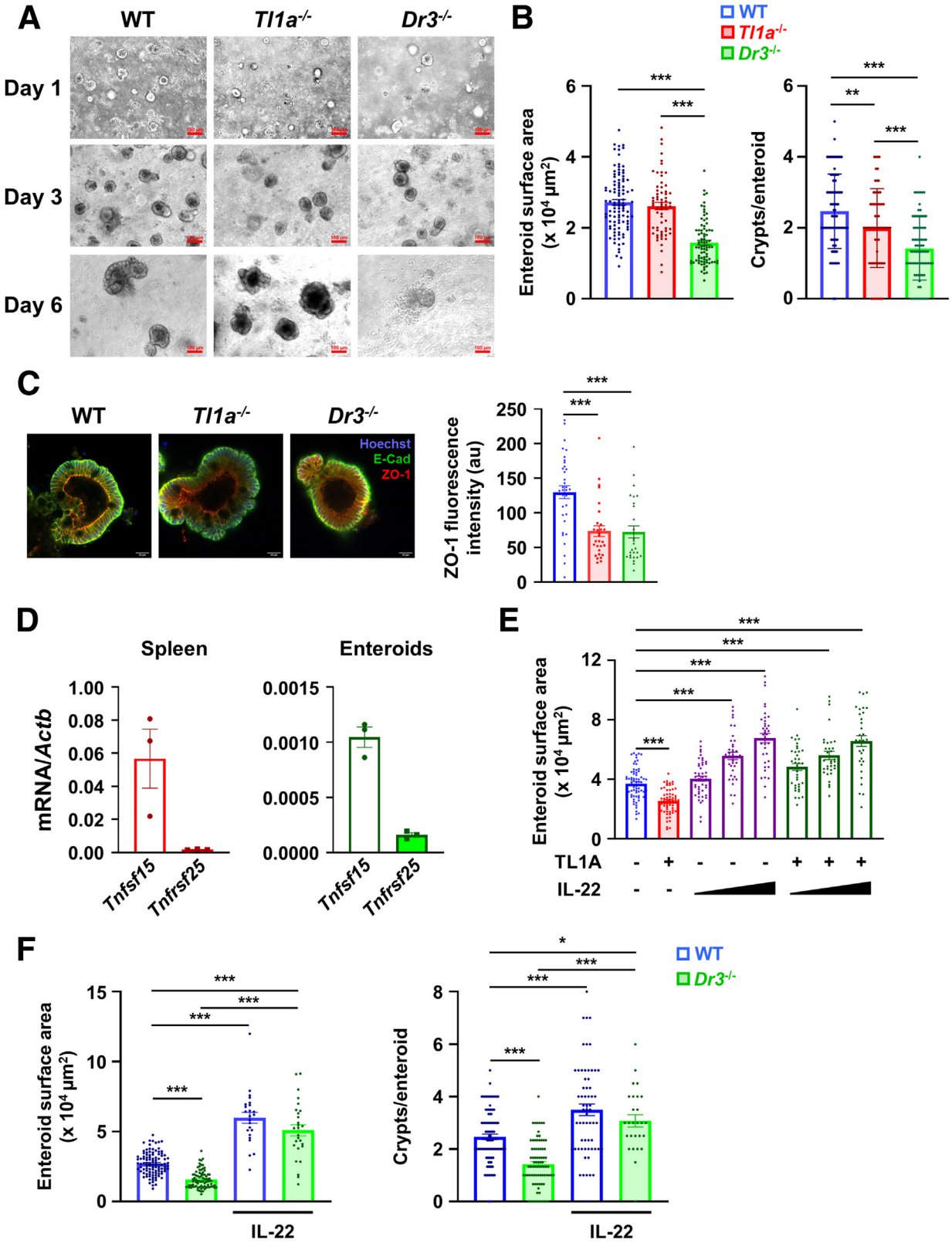


**Figure 8. DR3 but not TL1A deficiency results in impaired enteroid formation.** (*A*) Representative phase-contrast images of ileal enteroids developed from WT, *Tl1a*$^{-/-}$, and *Dr3*$^{-/-}$ mice captured on days 1, 3, and 6. *Scale bar*: 100 $\mu$m. (*B*) Quantification of enteroid surface area (*left*), and crypts/enteroid (*right*). (*C*) Representative images of ZO-1 (red), Hoechst dye (blue), and E-cadherin (green) immunofluorescence staining in WT, *Tl1a*$^{-/-}$, and *Dr3*$^{-/-}$ enteroids (*left*), and quantification of ZO-1 fluorescence intensity. *Scale bar*: 20 $\mu$m. At least 28 enteroids/genotype were analyzed. (*D*) mRNA expression of *Tnfsf15* and *Tnfrsf25* in spleen and enteroids was assessed by quantitative polymerase chain reaction (N = 3). (*E*) Quantification of enteroid surface area of WT enteroids treated with TL1A (100 ng/mL) and IL22 (0.25, 0.5, 1 ng/mL). (*F*) Quantification of enteroid surface area (*left*) and crypts/enteroid (*right*) of WT and *Dr3*$^{-/-}$ enteroids treated with or without IL22 (1 ng/mL). At least 13 enteroids/condition were analyzed. Three independent experiments were performed. Means ± SEM are shown. *$P < .05$, **$P < .01$, and ***$P < .005$. E-cad, E-cadherin.

mice has an impact on intestinal homeostasis that renders these mice more susceptible to colitis. Our data support this hypothesis by showing that deficiency of DR3 on IECs plays an essential role in impaired barrier function under homeostatic conditions and impaired IEC repair after tissue injury.

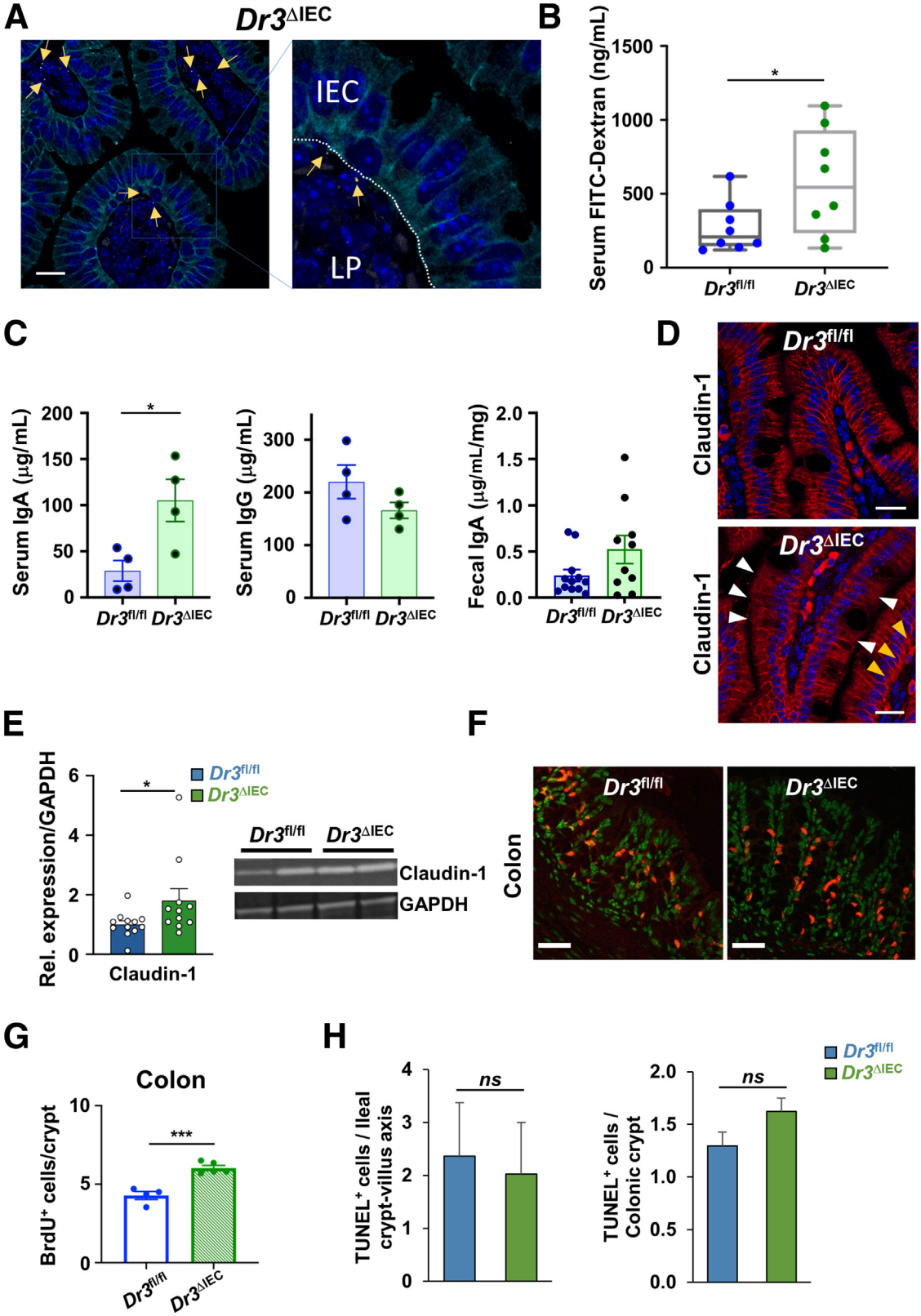

Although we observed a reduced frequency of Tregs in *Dr3*$^{-/-}$ mice that was consistent with a previous report using the acute DSS-induced colitis model[20] and with an important function of DR3 on Treg expansion and function,[21,33] we did not observe any increase in T-cell–derived proinflammatory cytokines or significantly increased inflammatory infiltrates into the LP. Although we did not investigate the immunosuppressive properties of Tregs from *Dr3*$^{-/-}$ mice, a previous publication failed to detect functional impairment of Tregs from *Dr3*$^{-/-}$ mice in an adoptive transfer model.[20] Our data suggest that immune responses might play a secondary role in the exacerbation of DSS-induced colitis in *Dr3*$^{-/-}$ mice and that impaired IEC regeneration leads to the severe stool phenotype we observed.

Recent studies have reported an indirect effect of the TL1A/DR3 pathway on IEC regeneration by inducing IL22 by ILC3s and T-helper cells.[19,37] IL22 has been shown to have a profound effect on mucosal healing by inducing the production of antimicrobial peptides and the acute phase protein serum amyloid A.[38–40] Here, we report a direct and cell-intrinsic effect of DR3 expressed by IECs on maintaining intestinal barrier integrity under homeostatic conditions and promoting mucosal healing after injury. Using a highly specific and sensitive probe for *Dr3*, we detected *Dr3* mRNA expression on murine IECs by sm-FISH. Moreover, we also observed *Dr3* expression on human IECs in surgical mucosal sections of CD patients. Mice with a deletion of DR3 on IECs (*Dr3*$^{\Delta IEC}$) showed increased intestinal permeability and uncontrolled proliferation of IECs under homeostatic conditions that also was observed in *Dr3*$^{-/-}$ mice. Furthermore, we observed increased expression and altered cellular location of several tight junction proteins in these mice. Claudin-1 regulates IEC proliferation and its overexpression worsens DSS-induced colitis and impairs epithelial regeneration.[26] Our findings of dysregulated claudin-1 expression support the idea that *Dr3*$^{\Delta IEC}$ mice are more susceptible to DSS-induced colitis by modulating expression and cellular localization of tight junction proteins. Low-dose TL1A has been shown to induce MLCK2 mRNA and MLCK protein phosphorylation to regulate tight junctions in the human cancer coli-2 cell line via the phosphoinositide 3-kinases/serine-threonine kinase 1 signaling pathway.[41] Further studies are warranted to determine the signaling pathways downstream of DR3 in IECs leading to alteration in tight junction protein expression and localization. Although DR3 signaling has been reported to activate caspase 8 and induce apoptosis in certain cell types, we did not observe any differences in IEC cell death in *Dr3*$^{\Delta IEC}$ mice. These data suggest that IEC cell death does not contribute to the compromised barrier function in *Dr3*$^{\Delta IEC}$ mice under homeostatic conditions.

Epithelial regeneration and wound repair are dependent on the self-renewal, proliferation, and differentiation of intestinal stem cells.[42] We observed significant growth defects, impairment of crypt formation, and compromised ZO-1 staining in *Dr3*$^{\Delta IEC}$ enteroids, highlighting the novel role of DR3 in the regulation of intestinal stem cell regenerative potential during homeostasis. We confirmed a direct effect of TL1A–DR3 signaling on enteroids and observed that TL1A stimulation leads to significant growth defects of WT enteroids. Our ex vivo data of impaired organoid formation of *Dr3*$^{\Delta IEC}$ enteroids and our observation that TL1A treatment of WT enteroids results in decreased enteroid surface area and crypts/enteroids are consistent with our in vivo data of impaired induction of IEC regeneration in *Dr3*$^{\Delta IEC}$ mice after DSS-induced injury and indicate impaired proliferation and differentiation in the absence of DR3 signaling in IECs. Although TL1A and IL22 have opposing effects on enteroid growth, our data suggest that IL22 prevents the inhibitory effects TL1A has on organoid formation and growth.

Intestinal microbiota contributes significantly to the inflammation seen in DSS-induced colitis. To exclude an impact of differences in intestinal microbiota on the susceptibility and severity of DSS colitis in our mice, we cohoused all experimental mice before and during DSS colitis. Nevertheless, we observed significant translocation of intestinal bacteria to MLNs in *Dr3*$^{\Delta IEC}$ mice that was not observed in WT mice and is consistent with the systemic inflammation that we observed in *Dr3*$^{\Delta IEC}$ mice. To determine if the increase in homeostatic IEC proliferation in *Dr3*$^{-/-}$ or *Dr3*$^{\Delta IEC}$ mice was microbiota-dependent, we treated *Dr3*$^{-/-}$ or *Dr3*$^{\Delta IEC}$ mice with broad-spectrum antibiotics and assessed BrdU incorporation. We did not observe any significant differences in the numbers of proliferating IECs in the ileum or colon of antibiotic-treated *Dr3*$^{-/-}$ or

**Figure 9.** (***See previous page***). **Intestinal epithelial DR3 promotes the integrity of the intestinal barrier and regulates IEC proliferation.** (*A*) Ileal villi on *Dr3*$^{\Delta IEC}$ mice were stained by sm-FISH. *Dr3* (yellow), DAPI (blue), and E-cadherin (cyan). *Arrows* point to LP cells expressing *Dr3* mRNA. *Dashed line* indicates the border between the IEC layer and LP. *Scale bar*: 20 $\mu$m. (*B*) *Dr3*$^{fl/fl}$ and *Dr3*$^{\Delta IEC}$ mice were gavaged with FITC-dextran. The FITC-dextran serum concentration was measured 1 hour postgavage. Data are shown as median with interquartile range. Each *dot* represents an individual mouse. (*C*) Serum IgA (*left*), IgG (*middle*), and fecal IgA (*right*) concentrations were measured in untreated *Dr3*$^{fl/fl}$ and *Dr3*$^{\Delta IEC}$ mice. (*D*) Representative ileal images of immunofluorescence of claudin-1 (red) and DAPI (blue) staining in *Dr3*$^{fl/fl}$ (*left*) and *Dr3*$^{\Delta IEC}$ (*right*) mice. *White arrowheads* indicate discontinuous claudin-1 staining at the apical side of the IEC layer. *Yellow arrowheads* indicate basolateral claudin-1 staining. *Scale bar*: 20 $\mu$m. (*E*) Protein expression of claudin-1 was assessed by Western blot. Relative expression is shown (*left*; N = 11–12/genotype). Representative images of Western blot (*right*). (*F* and *G*) *Dr3*$^{fl/fl}$ and *Dr3*$^{\Delta IEC}$ mice were injected intraperitoneally with BrdU 24 hours before being killed. (*F*) Representative colonic BrdU staining (red) co-stained with DAPI (green) are shown. *Scale bar*: 50 $\mu$m. (*G*) Quantification of BrdU$^+$ cells in colonic tissue sections. BrdU$^+$ cells were counted in 20 well-oriented crypts. Each *dot* represents the average BrdU$^+$ cells/crypts of an individual mouse. (*H*) Untreated *Dr3*$^{fl/fl}$ and *Dr3*$^{\Delta IEC}$ mice were assessed for TUNEL positivity in IECs. TUNEL$^+$ cells per ileal crypt–villus axis (*left*) and TUNEL$^+$ cells per colonic crypts (*right*). Means ± SEM are shown. *$P < .05$ by (*E* and *G*) Mann–Whitney *U* test or (*B*, *C*, and *H*) Student *t* test. GAPDH, glyceraldehyde-3-phosphate dehydrogenase; Rel, relative. ***$P < .005$

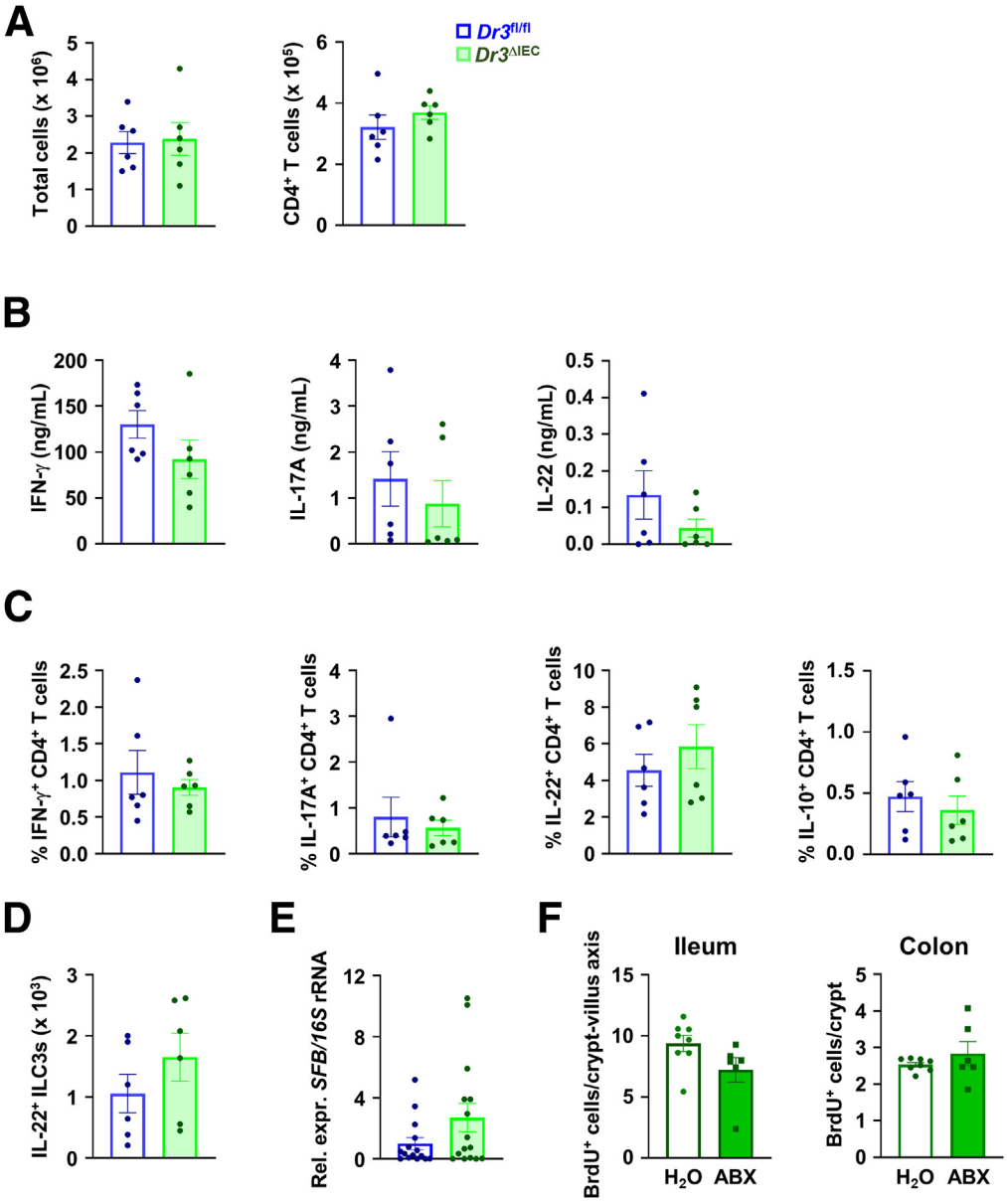


**Figure 10. $T_H1$, $T_H17$, and ILC3 responses were not altered in *Dr3*$^{\Delta IEC}$ mice.** Homeostatic immune profiles of 6- to 8-week-old *Dr3*$^{fl/fl}$ and *Dr3*$^{\Delta IEC}$ mice were analyzed. (*A*) Cells were isolated from LP and the total number of cells (*left*) and CD4$^+$ T cells (*right*) was counted. (*B*) Enzyme-linked immunosorbent assay analysis of IFN-gamma, IL17A, and IL22 production from LPMCs after ex vivo restimulation with anti-CD3 and anti-CD28. (*C*) Frequency of IFN-gamma, IL17A, IL22, and IL10-positive cells in LPMCs isolated from the large intestine were assessed by intracellular staining using flow cytometry. (*D*) Total numbers of IL22-positive ROR$\gamma$t$^+$ ILC3s in LPMCs isolated from the large intestine. (*E*) Quantification of relative abundance of *SFB* in fecal samples of co-housed 6- to 10-week-old *Dr3*$^{fl/fl}$ and *Dr3*$^{\Delta IEC}$ mice by quantitative polymerase chain reaction (N = 15/genotype). (*F*) *Dr3*$^{\Delta IEC}$ mice were treated with or without broad-spectrum antibiotics for 4 weeks. Quantification of BrdU$^+$ cells in tissue sections. BrdU$^+$ cells were counted in 20 well-oriented crypt–villi axis. Each *dot* represents the average of BrdU$^+$ cells/crypt–villi axis of an individual mouse. Means ± SEM are shown. ABX, antibiotics; rRNA, ribosomal RNA.

*Dr3*$^{\Delta IEC}$ mice compared with water controls, suggesting that the differences in homeostatic IEC proliferation in *Dr3*$^{-/-}$ or *Dr3*$^{\Delta IEC}$ mice are microbiome-independent.

Our data show a discrepancy of the response to acute DSS between *Dr3*$^{-/-}$ and *Tl1a*$^{-/-}$ mice that has been reported previously in these mice.[20] Although *Dr3*$^{-/-}$ mice present with impaired epithelial barrier integrity, altered expression and localization of tight junction proteins, and increased homeostatic proliferation, *Tl1a*$^{-/-}$ mice are similar to WT mice. One possible explanation that has been suggested is the presence of additional DR3 ligands, and some potential ligands have been identified in in vitro assays and in vivo models.[43–45] However, their contribution to acute intestinal inflammation remains elusive. Nevertheless, the similar phenotypes of complete *Dr3*$^{-/-}$ mice and *Dr3*$^{\Delta IEC}$ mice in regard to their IEC function suggests a key role of DR3 on

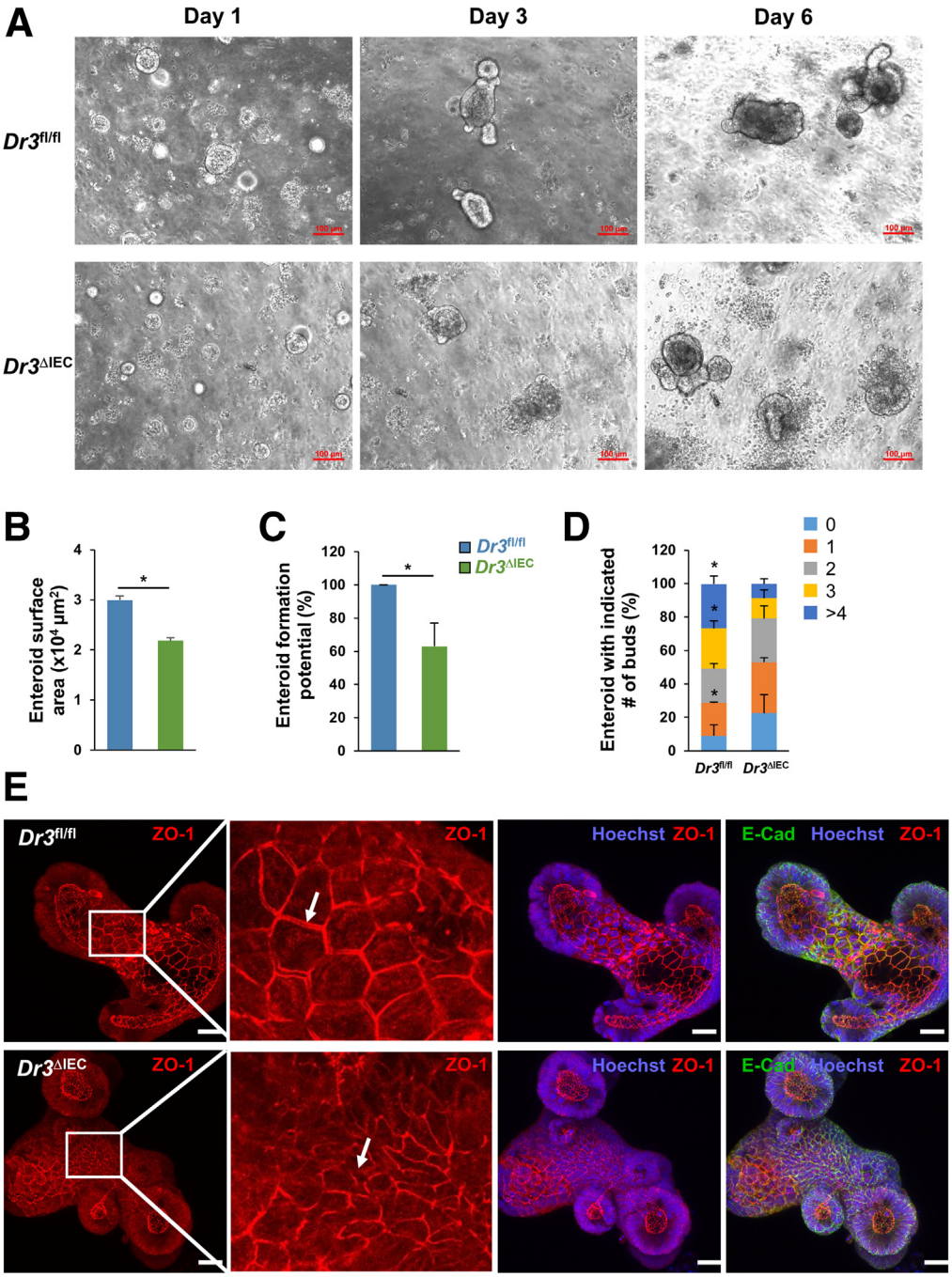


**Figure 11. Loss of DR3 in IECs leads to growth defects in enteroid cultures.** (*A*) Representative phase-contrast images of ileal enteroids developed from *Dr3*$^{fl/fl}$ and *Dr3*$^{\Delta IEC}$ mice captured on days 1, 3, and 6. *Scale bar*: 100 $\mu$m. (*B–D*) Enteroid-forming capacity of *Dr3*$^{fl/fl}$ and *Dr3*$^{\Delta IEC}$ crypts analyzed on day 6. (*B*) Enteroid surface area. (*C*) Percentage of enteroid formation potential. (*D*) De novo crypt formation (budding). (*E*) Representative images of ZO-1 (red), Hoechst dye (blue), and E-cadherin (green) immunofluorescence staining in *Dr3*$^{fl/fl}$ (*top*) and *Dr3*$^{\Delta IEC}$ (*bottom*) enteroids. *White arrows* indicate continuous and discontinuous ZO-1 staining on the luminal side of *Dr3*$^{fl/fl}$ and *Dr3*$^{\Delta IEC}$ enteroids, respectively. *Scale bars*: 20 $\mu$m. Three independent experiments were performed. Means ± SEM are shown. *$P < .05$.

IECs in maintaining homeostatic barrier function and mucosal healing after injury. Further studies using cell-type–specific deletions of TL1A are warranted to elucidate the complex functional network of the TL1A–DR3 pathway, including potential pleiotropic effects of TL1A on different cell types. One limitation of our study was the use of the acute DSS model, which is widely used in the field as an epithelial injury/repair model, but it does not reflect all aspects of human IBD or, more specifically, human ulcerative colitis. However, this model is useful in elucidating mechanisms of IEC regeneration or failure thereof as seen in ulcerative colitis. Our data showed that DR3 is expressed in mouse and human IECs. In addition to the known IBD risk loci in TL1A (*TNFSF15*), DR3 (*TNFRSF25*) has been identified recently as an IBD risk loci in a meta-analysis, supporting the importance of our findings.[10]

In conclusion, our findings uncovered a novel molecular mechanism underlying the intestinal pathology mediated through DR3 signaling specifically in IECs. These findings provide new insights into the mechanism of the TL1A–DR3

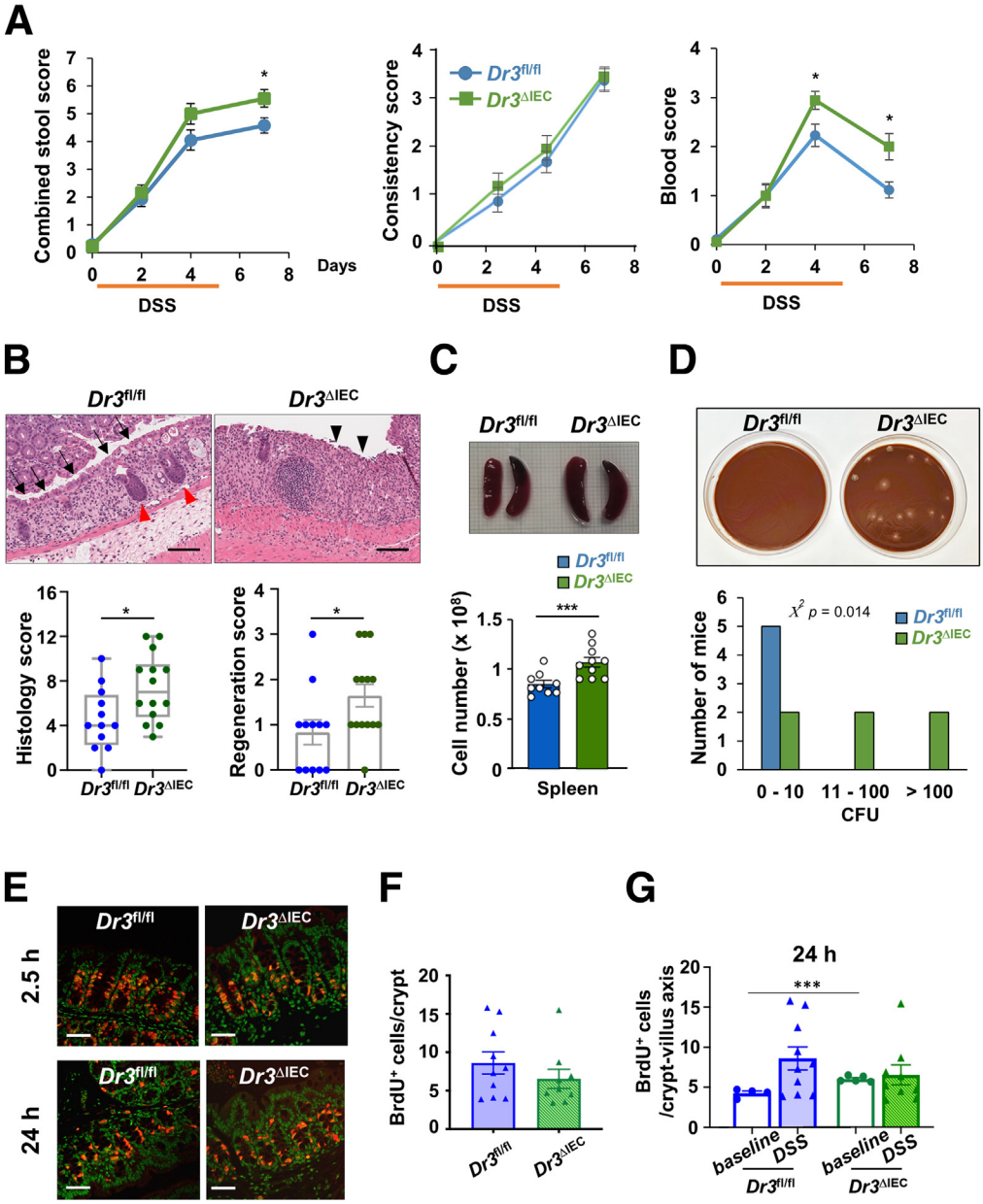


**Figure 12. Intestinal epithelial DR3 promotes tissue repair after DSS-induced injury.** *Dr3*$^{fl/fl}$ and *Dr3*$^{\Delta IEC}$ mice were treated with 3% DSS for 5 days to induce acute colitis. (*A*) Combined stool scores (*left*), consistency score (*middle*), and blood score (*right*) during acute DSS colitis (N = 17–18/genotype). (*B*) Representative H&E staining of *Dr3*$^{fl/fl}$ and *Dr3*$^{\Delta IEC}$ mouse rectal tissue (*top*). *Red arrowheads* indicate regenerating crypts, *black arrows* indicate regenerating epithelial layer, and *black arrowheads* indicate ulcerations. Histology score (*bottom left*), and regeneration score (*bottom right*) in rectum are shown. Each *dot* represents an individual mouse. Data are presented as median with interquartile range. *Scale bar*: 100 $\mu$m. (*C*) Representative macroscopic images of spleens (*top*) and splenocyte numbers (*bottom*) from 2 independent experiments are shown (N = 9–10/genotype). (*D*) MLN homogenates were cultured under anerobic conditions on chocolate blood agar plates. Representative images for colonies (*top*). Colony forming unit (CFU) was analyzed by $X^2$ test (N = 5–6/genotype) (bottom). (*E* and *F*) *Dr3*$^{fl/fl}$ and *Dr3*$^{\Delta IEC}$ mice were injected intraperitoneally with BrdU 24 hours before being killed. (*E*) Representative colonic BrdU staining (red) co-stained with DAPI (green). *Scale bar*: 50 $\mu$m. (*F*) Quantification of BrdU$^+$ cells in colonic tissue sections. BrdU$^+$ cells were counted in 20 well-oriented crypts. Each symbol represents the average BrdU$^+$ cells/crypt of an individual mouse. (*G*) Quantification of BrdU$^+$ cells in colonic tissue sections of water and DSS-treated mice. BrdU$^+$ cells were counted in 20 well-oriented crypt–villi axis. Each symbol represents the average of BrdU$^+$ cells/crypt–villi axis of an individual mouse. Means ± SEM are shown. *$P < .05$, ***$P < .005$.

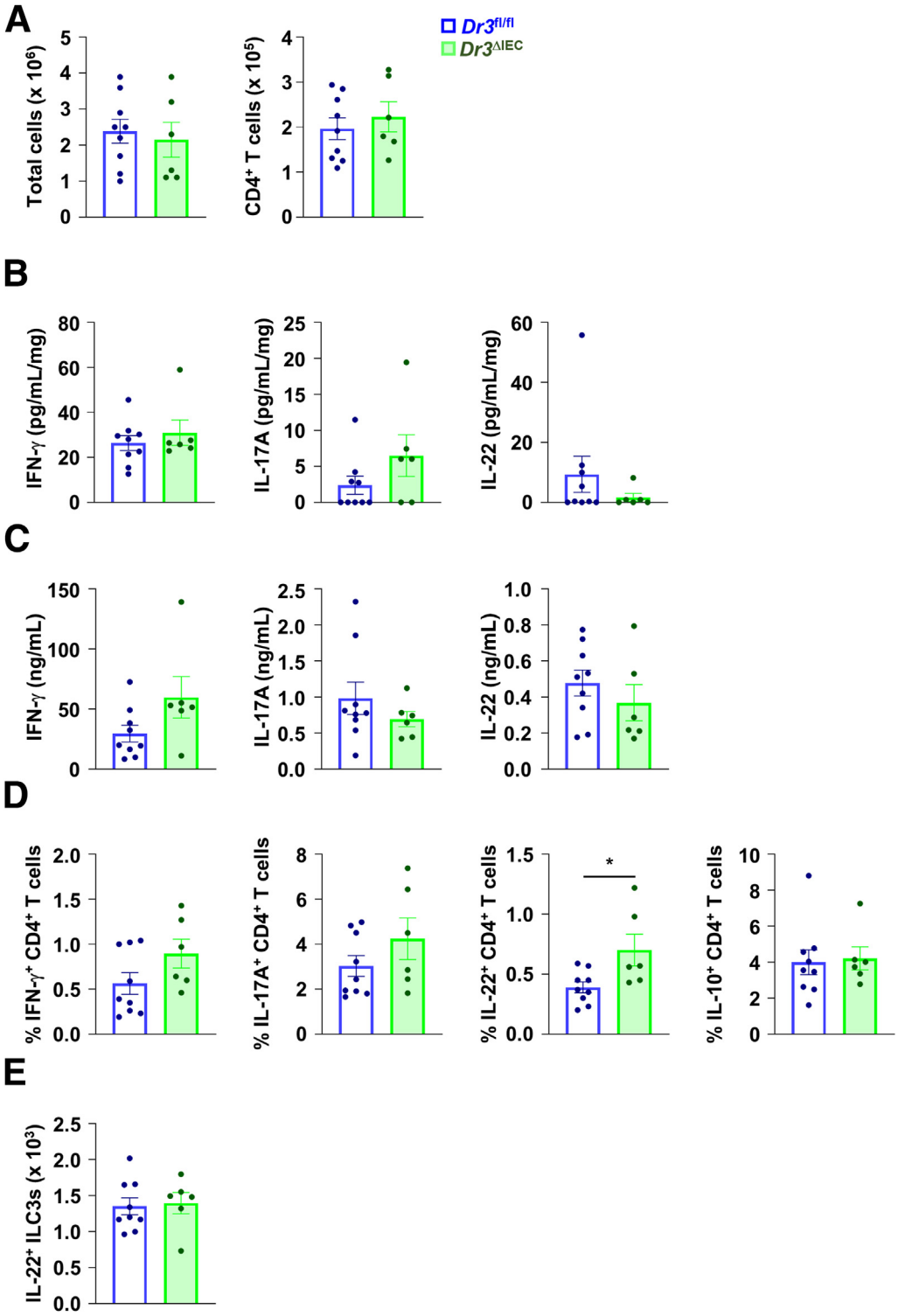


**Figure 13. $T_H1$, $T_H17$, and ILC3 responses are not altered in *Dr3*$^{\Delta IEC}$ mice during acute DSS colitis.** *Dr3*$^{fl/fl}$ and *Dr3*$^{\Delta IEC}$ mice were treated with 3% DSS for 3 days to induce acute colitis. (*A*) Cells were isolated from LP and the total number of cells (*left*) and CD4$^+$ T cells (*right*) were counted. (*B*) Ileal tissue explants were cultured for 24 hours and supernatants were analyzed by enzyme-linked immunosorbent assay (ELISA). Concentrations of secreted cytokines were normalized to the dry weight of the tissue sections. (*C*) ELISA analysis of IFN-gamma, IL17A, and IL22 production from LPMCs after ex vivo restimulation with anti-CD3 and anti-CD28. (*D*) Frequency of IFN-gamma, IL17A, IL22, and IL10-positive cells in LPMCs isolated from the large intestine were assessed by intracellular staining using flow cytometry. (*E*) Total number of IL22-positive RORγt$^+$ ILC3s in LPMCs isolated from the large intestine. Each *dot* represents an individual mouse. Means ± SEM are shown. *$P < .05$.

pathway in the pathogenesis of IBD and suggest that therapeutic approaches targeting TL1A rather than DR3 could provide anti-inflammatory therapy while preserving the repair mechanisms downstream of DR3 in IECs.

# Methods

## Antibodies and Reagents

The following primary antibodies were used: anti–E-cadherin (1:100, cat. Asp155-Ile707; R&D Systems, Minneapolis, MN), anti-BrdU (1:100, cat. BU1/75 [ICR1]; NOVUS Biologicals, Centennial, CO), anti–ZO-1 (1:100, cat. 61-7300; Thermo Fisher Scientific, Waltham, MA), anti–claudin-1 (1:200, cat. ab15098; Abcam, Waltham, MA), anti–claudin-2 (1:200, cat. ab53032; Abcam), and anti–occludin-1 (1:50, cat. 40-4700; Thermo Fisher Scientific). The following secondary antibodies were used: anti-goat (1:500, A11058; Life Technology, Carlsbad, CA), anti-rat (1:500, cat. ab150160; Abcam), and anti-rabbit (1:500, cat. A-11037; Thermo Fisher Scientific). 4',6-diamidino-2-phenylindole (cat. 0100-20; Southern Biotech, Birmingham, AL) was used for counterstaining for immunofluorescence and FISH. Fluorophore-conjugated antibodies against CD4 (GK1.5, RM4-5), CD45 (30-F11), CD90.2 (53-2.1), CD127 (A7R34), IFN-gamma (XMG1.2), IL17A (TC11-18H10.1), and corresponding isotype controls were from BioLegend (San Diego, CA), and antibodies against FoxP3 (FJK-16s), IL22 (1H8PWSR), RORγt (B2D), Natural Killer Cell P46-Related Protein (29A1.4), hematopoietic lineage cocktail (88-7772-72), IL10 (JES5-16E3), and corresponding isotype controls were from Thermo Fisher Scientific.

## Mice

Tl1a-deficient (*Tl1a*$^{-/-}$), Dr3-deficient (*Dr3*$^{-/-}$), and mice with a floxed Dr3 allele (*Dr3*$^{fl/fl}$) on a C57BL/6J background were generated as previously described.[18] Villin-Cre mice were purchased from Jackson Laboratory and crossed with *Dr3*$^{fl/fl}$ to generate *Dr3*$^{\Delta IEC}$ mice. All mice were maintained under specific pathogen-free conditions and handled according to the guidelines and approved protocols of the Cedars-Sinai Medical Center Animal Care and Use Committee (protocol 7430, 8793). Littermates were co-housed throughout the length of the experiments. Female age-matched mice were used for the DSS-induced colitis model, intestinal permeability assay, and assessment of the expression of tight junction genes/proteins.

## Acute and Chronic DSS-Induced Colitis Model

Female 8- to 12-week-old mice were used for DSS-induced colitis. DSS (40,000–50,000 molecular weight) (cat. 160110; MP Biomedicals, Irvine, CA) was added to the drinking water at a concentration of 2.5% and given ad libitum on days 1–5, 8–12, 15–19, and 22–26 for the induction of chronic colitis, and 3% on days 1–5 for the induction of acute colitis. Body weights and disease activity index were monitored 3 times a week. The disease activity index was scored and calculated as described using freshly collected stool to determine the stool scores.[18] In brief, the combined stool scores were calculated by adding the stool consistency score (0, firm dry stool; 1, moist stool; 2, soft adherent stool; 3, large soft pliable stool; and 4, liquid stool) and the stool blood score (0, no color; 1, flecks of blue; 2, up to 50% blue; 3, >50% blue; and 4, gross red blood). The amount of blood in the stool was quantified using Hemoccult Sensa tests (cat. 64151; Beckman Coulter, Brea, CA). Mice were killed on day 29 for the chronic model and on day 8 for the acute model.

## Depletion of Gut Microbiota by Antibiotic Treatment

Mice received antibiotic treatment from the time of weaning until 8 weeks of age. A combination of 4 antibiotics (1 g/L ampicillin, 500 mg/L vancomycin, 1 g/L neomycin sulfate, and 1 g/L metronidazole) was added to the drinking water and changed once per week.

## Histology Scoring

Intestinal tissues were fixed in 10% neutral buffered formalin, embedded in paraffin, and stained with H&E for histologic analysis. Histopathologic scores were assigned in a blinded manner by 2 trained animal pathologists as previously described and the average of both scores was reported.[11,46] In brief, the chronic DSS model was scored as follows: inflammation: 0, none; 1, mild; 2, moderate; and 3, severe; extent: 0, none; 1, mucosa; 2, mucosa and submucosa; and 3, transmural; regeneration: 0, complete regeneration; 1, almost complete regeneration; 2, regeneration with crypt depletion; 3, surface epithelium not intact; and 4, no tissue repair; crypt damage: 0, none; 1, basal one-third damaged; 2, basal two-thirds damaged; 3, only surface epithelium intact; and 4, entire crypt and epithelium lost; and percentage involvement: 1, 1% to 25%; 2, 26% to 50%; 3, 51% to 75%; and 4, 76% to 100%. The total histology score is given as inflammation + extent + regeneration + crypt damage + percentage involvement.[11] Acute DSS colitis was scored as described.[46]

## Cell Isolation and Culture

Colons were excised swiftly and opened longitudinally, followed by washing with PBS. Epithelial cells were scraped off with a glass slide and collected for RNA isolation or protein extraction. LPMCs were isolated as previously described.[17]

## Flow Cytometric Analysis

Cells were restimulated with 50 ng/mL phorbol 12-myristate 13-acetate, 500 ng/mL ionomycin, and Monensin (cat. 00-4505; Thermo Fisher Scientific) for 4 hours, stained with live/dead dye (Thermo Fisher Scientific) and anti-CD4, fixed and permeabilized using the FoxP3 staining buffer set (Thermo Fisher Scientific), and stained with antibodies against murine IL17A, IFN-gamma, IL10, IL22, and FoxP3. For ILC3 staining, cells were stimulated with IL23 (40 ng/mL), IL1$\beta$ (100 ng/mL), and Brefeldin A for 4 hours, and then stained with hematopoietic lineage cocktail and antibodies against murine Natural Killer Cell P46-Related Protein, IL22, RORγt, CD45, CD90.2, and CD127. The following gating strategy was used to analyze ILC3: immune cells were gated based on forward and side scatter, excluding

cell aggregates. Then, ILC3 was identified as $CD45^{+}$ $Lin^{-}$ $CD127^{+}$ $CD90.2^{High}$ $Ror\gamma t^{+}$ $IL22^{+}$. Samples were acquired using a LSRII flow cytometer (BD Biosciences, Franklin Lakes, NJ) or the Sony ID7000 Spectral Cell Analyzer and analyzed using FlowJo software (TreeStar, Inc, Ashland, OR).

## Enzyme-Linked Immunosorbent Assay

Blood was collected by retro-orbital bleeding and serum was stored at -80ºC until use. Serum IgA (cat. 88-50450) and IgG (cat. 88-50400, both Thermo Fisher Scientific) were assayed by enzyme-linked immunosorbent assay according to the manufacturer's instructions.

## Quantification of Fecal IgA

Fecal pellets were collected from 8-week-old *Dr3*$^{fl/fl}$ and *Dr3*$^{\Delta IEC}$ mice and reconstituted in 1 mL phosphate-buffered saline (PBS) containing 1% bovine serum albumin (BSA) (w/v) overnight at 4ºC. Samples were processed as described.[47] In brief, cell-free supernatants of fecal matter were used for IgA enzyme-linked immunosorbent assay. Secreted IgA concentrations were normalized to the total weight of fecal pellets.

## Intestinal Permeability Assay

Eight-week-old female mice were fasted overnight and orally gavaged with FITC-dextran (molecular weight, 3000–5000 daltons, Sigma; 500 mg/kg body weight). Blood was collected by retro-orbital bleeding 1 hour after gavage and serum was obtained and stored at -80ºC until use. The serum FITC-dextran concentration was measured with a fluorescence spectrophotometer (SpectraMax; Molecular Devices) at an excitation/emission of 485 nm/520 nm and analyzed using a standard curve of FITC dextran diluted in PBS. Mouse serum from untreated mice was used as a background control.

## Enteroid Culture

The enteroid culture was performed using the ileal crypts isolated from *Dr3*$^{fl/fl}$ and *Dr3*$^{\Delta IEC}$ mice as described previously.[48] Briefly, the ileum was collected, washed in ice-cold Dulbecco's phosphate-buffered saline (DPBS) without $Ca^{2+}$ and $Mg^{2+}$, cut open vertically, and luminal content was washed out with ice-cold DPBS. Tissue pieces (2–3 mm) were washed in DPBS and incubated for 20 minutes at room temperature in DPBS/2 mmol/L EDTA with agitation. After the intestinal pieces settled down, DPBS/EDTA buffer was replaced with DPBS/0.1% BSA, gently vortexed for 30–60 seconds, and filtered through a 70-$\mu$m cell strainer to remove the tissue chunks. This step was repeated 2 more times and a total of 3 fractions were collected. Fractions 2 and 3 were pooled, centrifuged at 290 $\times$ $g$ for 5 minutes, 4ºC, and washed with DPBS/0.1% BSA by centrifuging at 200 $\times$ $g$ for 3 minutes, 4ºC. Crypts then were resuspended in Advanced Dulbecco's modified Eagle medium/F12 (12034; Gibco). Epidermal growth factor (EGF)/Noggin/R-spondin-1 (ENR) media (Advanced Dulbecco's modified Eagle medium/F12, 10 mmol/L HEPES, 1$\times$ GlutMAX supplement, 100 U/mL penicillin/streptomycin, 1 mmol/L N-acetylcysteine (A9165; Sigma Aldrich), 1 $\times$ B-27 supplement (17504; Life Technologies), 1 $\times$ N-2 supplement (17502; Thermo Fisher Scientific), 50 ng/mL recombinant human epidermal growth factor (AF10015), 100 ng/mL recombinant murine noggin (20538), 1 $\mu$g/mL recombinant human R-spondin-1 (12038; all Peprotech, Rocky Hill, NJ)), and Matrigel 1:1 (356231; Corning, Corning, NY) were added to the crypts at a seeding density of 100 crypts per 20 $\mu$L. Cell suspension (20 $\mu$L) was added to a single well of a 48-well plate (pre-incubated for 30 minutes at 37ºC) and incubated for 10 minutes at 37ºC for polymerization and dome formation. After polymerization of Matrigel, 250 $\mu$L ENR media was added to each well. The medium was replaced every 2–3 days with fresh media. Images were acquired using a Zeiss Axio Observer.Z1 inverted microscope at 10$\times$ magnification on days 1, 3, and 6. On day 1, enteroids were treated with either TL1A (1896; R&D Systems) or IL22 (Peprotech). RNA from organoids was extracted by adding RNA lysis buffer lysis buffer (Qiagen) directly to the enteroids on day 6 of culture and following the manufacturer's instructions. The day 6 images were used for the quantification of enteroid surface area and counting the buds/crypts. For enteroid formation potential, the live, intact, and viable enteroids were counted on day 6 and then normalized to the counted enteroids on day 1 of the same well. At least 70–120 enteroids were included in the analysis. The enteroid surface area was calculated using ZEN2 software (Carl Zeiss microscopy).

## Immunofluorescence and Confocal Microscopy

Intestines were excised from 8-week-old mice and immediately fixed in 10% neutral buffered formalin followed by paraffin-embedding. Tissue sections were deparaffinized, boiled in citrate buffer (10 mmol/L sodium citrate, 0.05% Tween-20; pH 6.0) for antigen retrieval, and incubated with primary antibodies overnight. Fluorophore-conjugated secondary antibodies were incubated for 1 hour. Images were captured with a TCS SP5 X confocal microscope (Leica) and analyzed using LAS AF Lite software (Leica). BrdU-positive cells were counted in a well-oriented crypt–villi axis by an observer blinded to the genotypes. Whole-mount enteroid staining was performed as previously described.[49] Briefly, enteroids were fixed in 4% paraformaldehyde, blocked with PBS/0.1% Triton X-100/0.2% BSA (enteroid wash buffer), and incubated with rabbit anti–ZO-1 (1:100, 61-7300; Thermo Fisher Scientific) and goat anti–E-cadherin (1:200, AF648; R&D Systems) antibodies overnight at 4°C. The enteroids were incubated overnight with donkey anti-goat AF 594 (1:500, A11058; Life Technology) and donkey anti-rabbit Dylight 650 (1:500, ab96922; Abcam), followed by nuclei staining with Hoechst 33342 dye (62249; Thermo Fisher Scientific). The enteroids were mounted on glass slides using fructose–glycerol solution. Images were acquired using a Leica Stellaris 8 confocal microscope and analyzed using ImageJ software (Fiji).

## TUNEL Assay

For cell death detection, the TUNEL assay was performed using the Click-iT Plus TUNEL assay kit according to

the manufacturer's instructions (C10618; Thermo Fisher Scientific). Fixed ileal and colonic tissues from *Dr3*$^{fl/fl}$ and *Dr3*$^{\Delta IEC}$ mice were used.

### sm-FISH

Tissues were prepared as described for immunofluorescence staining. The DR3 transcripts were detected using the RNAscope Multiplex Fluorescent Reagent Kit v2 (ACD, Newark, CA) according to the manufacturer's instruction followed by immunofluorescence staining for E-cadherin. The probe for murine *Dr3* transcripts was custom designed to hybridize between exons 2 and 5 of murine *Dr3*, which was deleted in the process of generating *Dr3*$^{-/-}$ mice. Probes for Peptidylprolyl Isomerase B (Cyclophilin B) and Hela cell pellets were used as quality controls in this assay and a probe for Bacillus subtilis dihydrodipicolinate reductase was used as a negative control. The probe for human DR3 was purchased from Advanced Cell Diagnostics (cat. 448571). Deidentified formalin-fixed, paraffin-embedded tissue taken from the unaffected margin of small-bowel tissue resected during small-bowel resection for complicated CD was used. Tissue samples were obtained by the Material and Information Resources for Inflammatory and Digestive Diseases IBD Biobank after the patients' informed consent and approval by the Institutional Review Board of the Cedars-Sinai Medical Center (protocol #3358).

### RNA, DNA Isolation, and Quantitative Polymerase Chain Reaction

RNA was extracted from isolated epithelial cells using RNeasy Mini Kit (Qiagen, Germantown, MD) and complementary DNA was synthesized using the Omniscript RT kit (Qiagen). Complementary DNA was amplified with the QuantiTect SYBR Green Polymerase Chain Reaction Kit (Qiagen) and specific primers using Eppendorf MasterCycler RealPlex (Eppendorf, Enfield, CT). Fecal samples were collected from 8-week-old mice, snap-frozen, and stored at -80°C. DNA was isolated using the DNeasy PowerSoil DNA Isolation Kit (Qiagen) following the manufacturer's instructions. The abundance of SFB was measured by quantitative polymerase chain reaction using 25 ng fecal bacterial DNA and specific 16S ribosomal RNA primers for SFB. The relative abundance for SFB was quantified by normalizing the quantity of SFB 16S ribosomal RNA gene to the total amount of 16S bacterial DNA. Sequences of primers used in this study were as follows: *Gapdh* sense: 5'-ACAG TCCATGCCATCACTGCC-3', antisense: 5'-GCCTGCTTCACCAC CTTCTTG-3', *Atcb* sense: 5'-GACGGCCAGGTCATCACTATT-3', antisense: 5'-AGGAAGGCTGGAAAAGAGCC-3', *claudin-1* sense: 5'-CTGGAAGATGATGAGGTGCAGAAGA-3, antisense: 5'-CCAC-TAATGTCGCCAGACCTGAA-3', *claudin-2*: 5'-GGCTGTTAGGCA-CATCCAT-3', antisense: 5'-TGGCACCAACATAGGAACTC-3', *claudin-3* sense: 5'-AAGCCGAATGGACAAAGAA-3', antisense: 5'-CTGGCAAGTAGCTGCAGTG-3', *claudin-4* sense: 5'-CGCT ACTCTTGCCATTACG-3', antisense: 5'-ACTCAGCACACCATGA CTTG-3', *claudin-15* sense: 5'-CCACCAGGGCTGGGCTT-3', antisense: 5'-TCCTGGAGACAGTGGGACAA-3', *Mlck* sense: 5'-GGGAAGGCATCACTGAGGTTT-3', antisense: 5'-GCTCTCAG-CAGGCACAGGTGA-3', *Tnfsf15* sense 5'-CAGCAGAAGGATGG CAGAGG-3', antisense: 5'-CTCTGGCCTGTGTCTACAGC-3', *Tnfrsf25* sense: 5'-GCGTTCTTTGGGGCTATC-3', antisense: 5'-TCCCAG-TACTGCTTGGAGGT-3', *16S ribosomal RNA* universal primer sense: 5'-ACTCCTACGGGAGGCAGCAGT-3', antisense: 5'-ATTA CCGCGGCTGCTGGC-3', and *SFB* sense: 5'-GACGCTGAGGCATGA-GAGCAT-3', antisense: 5'-GACGGCACGGATTGTTATTCA-3'. Expression levels for each gene were normalized to that of the housekeeping genes *Gapdh* or *Actb* and calculated using the $2^{-\Delta\Delta CT}$ method.

### Protein Extraction and Western Blot

Isolated epithelial cells were washed with DPBS containing sodium orthovanadate and lysed in 50 mmol/L HEPES, 250 mmol/L NaCl, 20 mmol/L $\beta$-glycerophosphate, 1 mmol/L sodium orthovanadate, 1 mmol/L EDTA, 1% NP-40, and protease inhibitors (Calbiochem). Lysates were separated by sodium dodecyl sulfate–polyacrylamide gel electrophoresis through 14% Tris-glycine gels (Invitrogen), transferred to polyvinylidene difluoride membranes, blocked (Odyssey Blocking Buffer, cat. 927-70001; Li-COR Biosciences), and incubated with anti–claudin-1 (1:150), anti–claudin-2 (1:1000), or anti–glyceraldehyde-3-phosphate dehydrogenase (1:2500, ab9485; Abcam) overnight at 4ºC followed by incubation with IRDye goat anti-rabbit antibody (1:5000, cat. 926-32211; Li-COR Biosciences). Images were visualized with the Odyssey Infrared Imaging System (Li-COR Biosciences). Expression levels for each protein were analyzed using ImageJ software (National Institutes of Health, Bethesda, MD) and normalized to that of glyceraldehyde-3-phosphate dehydrogenase.

### Bacterial Cultures From MLNs

MLNs were homogenized in 500 $\mu$L prereduced sterile PBS using a disposable pellet pestle. A total of 100 $\mu$L homogenate was plated on prereduced chocolate blood agar. Growth was recorded 1 week out. Tissue processing and cultivation were performed anaerobically.

### Statistical Analysis

Data were analyzed using GraphPad Prism software (GraphPad Software, La Jolla, CA) or JMP pro13 (JMP Statistical Discovery) and presented as the means ± SEM. Differences between the 2 groups were analyzed using the unpaired, 2-tailed Student *t* test or the Mann–Whitney *U* test. Analysis of variance with the Tukey honestly significant difference test was used to analyze statistical significance for more than 2 groups. Chi-squared analysis was used to analyze bacterial translocation in *Dr3*$^{fl/fl}$ and *Dr3*$^{\Delta IEC}$ mice. *P* values less than .05 were considered statistically significant.

The graphical abstract was created with BioRender.

All authors had access to the study data and reviewed and approved the final manuscript.

## References

1. Maloy KJ, Powrie F. Intestinal homeostasis and its breakdown in inflammatory bowel disease. Nature 2011; 474:298–306.

2. Xavier RJ, Podolsky DK. Unravelling the pathogenesis of inflammatory bowel disease. Nature 2007;448:427–434.
3. Migone TS, Zhang J, Luo X, et al. TL1A is a TNF-like ligand for DR3 and TR6/DcR3 and functions as a T cell costimulator. Immunity 2002;16:479–492.
4. Papadakis KA, Zhu D, Prehn JL, et al. Dominant role for TL1A/DR3 pathway in IL-12 plus IL-18-induced IFN-gamma production by peripheral blood and mucosal CCR9+ T lymphocytes. J Immunol 2005;174:4985–4990.
5. Prehn JL, Thomas LS, Landers CJ, et al. The T cell costimulator TL1A is induced by FcgammaR signaling in human monocytes and dendritic cells. J Immunol 2007; 178:4033–4038.
6. Cleynen I, Boucher G, Jostins L, et al. Inherited determinants of Crohn's disease and ulcerative colitis phenotypes: a genetic association study. Lancet 2016; 387:156–167.
7. de Lange KM, Moutsianas L, Lee JC, et al. Genome-wide association study implicates immune activation of multiple integrin genes in inflammatory bowel disease. Nat Genet 2017;49:256–261.
8. Jostins L, Ripke S, Weersma RK, et al. Host-microbe interactions have shaped the genetic architecture of inflammatory bowel disease. Nature 2012; 491(7422):119–124.
9. Yamazaki K, McGovern D, Ragoussis J, et al. Single nucleotide polymorphisms in TNFSF15 confer susceptibility to Crohn's disease. Hum Mol Genet 2005;14:3499–3506.
10. Cordero RY, Cordero JB, Stiemke AB, et al. Trans-ancestry, Bayesian meta-analysis discovers 20 novel risk loci for inflammatory bowel disease in an African American, East Asian, and European cohort. Hum Mol Genet 2023;32:873–882.
11. Barrett R, Zhang X, Koon HW, et al. Constitutive TL1A expression under colitogenic conditions modulates the severity and location of gut mucosal inflammation and induces fibrostenosis. Am J Pathol 2012;180:636–649.
12. Michelsen KS, Thomas LS, Taylor KD, et al. IBD-associated TL1A gene (TNFSF15) haplotypes determine increased expression of TL1A protein. PLoS One 2009;4: e4719.
13. Richard AC, Peters JE, Savinykh N, et al. Reduced monocyte and macrophage TNFSF15/TL1A expression is associated with susceptibility to inflammatory bowel disease. PLoS Genet 2018;14:e1007458.
14. Meylan F, Song YJ, Fuss I, et al. The TNF-family cytokine TL1A drives IL-13-dependent small intestinal inflammation. Mucosal Immunol 2011;4:172–185.
15. Shih DQ, Barrett R, Zhang X, et al. Constitutive TL1A (TNFSF15) expression on lymphoid or myeloid cells leads to mild intestinal inflammation and fibrosis. PLoS One 2011;6:e16090.
16. Zheng L, Zhang X, Chen J, et al. Sustained Tl1a (Tnfsf15) expression on both lymphoid and myeloid cells leads to mild spontaneous intestinal inflammation and fibrosis. Eur J Microbiol Immunol 2013;3:11–20.
17. Takedatsu H, Michelsen KS, Wei B, et al. TL1A (TNFSF15) regulates the development of chronic colitis by modulating both T-helper 1 and T-helper 17 activation. Gastroenterology 2008;135:552–567.
18. Shih DQ, Zheng L, Zhang X, et al. Inhibition of a novel fibrogenic factor Tl1a reverses established colonic fibrosis. Mucosal Immunol 2014;7:1492–1503.
19. Castellanos JG, Woo V, Viladomiu M, et al. Microbiota-induced TNF-like ligand 1A drives group 3 innate lymphoid cell-mediated barrier protection and intestinal T cell activation during colitis. Immunity 2018; 49:1077–1089 e5.
20. Jia LG, Bamias G, Arseneau KO, et al. A novel role for TL1A/DR3 in protection against intestinal injury and infection. J Immunol 2016;197:377–386.
21. Sidhu-Varma M, Shih DQ, Targan SR. Differential levels of Tl1a affect the expansion and function of regulatory T cells in modulating murine colitis. Inflamm Bowel Dis 2016;22:548–559.
22. Bamias G, Filidou E, Goukos D, et al. Crohn's disease-associated mucosal factors regulate the expression of TNF-like cytokine 1A and its receptors in primary subepithelial intestinal myofibroblasts and intestinal epithelial cells. Transl Res 2017;180:118–130 e2.
23. Jacob N, Jacobs JP, Kumagai K, et al. Inflammation-independent TL1A-mediated intestinal fibrosis is dependent on the gut microbiome. Mucosal Immunol 2018; 11:1466–1476.
24. Citalan-Madrid AF, Vargas-Robles H, Garcia-Ponce A, et al. Cortactin deficiency causes increased RhoA/ROCK1-dependent actomyosin contractility, intestinal epithelial barrier dysfunction, and disproportionately severe DSS-induced colitis. Mucosal Immunol 2017; 10:1237–1247.
25. Laukoetter MG, Nava P, Lee WY, et al. JAM-A regulates permeability and inflammation in the intestine in vivo. J Exp Med 2007;204:3067–3076.
26. Pope JL, Bhat AA, Sharma A, et al. Claudin-1 regulates intestinal epithelial homeostasis through the modulation of Notch-signalling. Gut 2014;63:622–634.
27. Corredor J, Yan F, Shen CC, et al. Tumor necrosis factor regulates intestinal epithelial cell migration by receptor-dependent mechanisms. Am J Physiol Cell Physiol 2003;284:C953–C961.
28. Kaiser GC, Polk DB. Tumor necrosis factor alpha regulates proliferation in a mouse intestinal cell line. Gastroenterology 1997;112:1231–1240.
29. Su L, Nalle SC, Shen L, et al. TNFR2 activates MLCK-dependent tight junction dysregulation to cause apoptosis-mediated barrier loss and experimental colitis. Gastroenterology 2013;145:407–415.
30. Bamias G, Martin C 3rd, Marini M, et al. Expression, localization, and functional activity of TL1A, a novel Th1-polarizing cytokine in inflammatory bowel disease. J Immunol 2003;171:4868–4874.
31. Pappu BP, Borodovsky A, Zheng TS, et al. TL1A-DR3 interaction regulates Th17 cell function and Th17-mediated autoimmune disease. J Exp Med 2008; 205:1049–1062.
32. Richard AC, Tan CY, Hawley ET, et al. The TNF-family ligand TL1A and its receptor DR3 promote T cell-mediated allergic immunopathology by enhancing differentiation and pathogenicity of IL-9-producing T cells. J Immunol 2015;194:3567–3582.

33. Schreiber TH, Wolf D, Tsai MS, et al. Therapeutic Treg expansion in mice by TNFRSF25 prevents allergic lung inflammation. J Clin Invest 2010;120:3629–3640.
34. Tsuda M, Hamade H, Thomas LS, et al. A role for BATF3 in TH9 differentiation and T-cell-driven mucosal pathologies. Mucosal Immunol 2019;12:644–655.
35. Hedl M, Abraham C. A TNFSF15 disease-risk polymorphism increases pattern-recognition receptor-induced signaling through caspase-8-induced IL-1. Proc Natl Acad Sci U S A 2014;111:13451–13456.
36. Wen L, Zhuang L, Luo X, et al. TL1A-induced NF-kappaB activation and c-IAP2 production prevent DR3-mediated apoptosis in TF-1 cells. J Biol Chem 2003;278:39251–39258.
37. Thomas LS, Targan SR, Tsuda M, et al. The TNF family member TL1A induces IL-22 secretion in committed human Th17 cells via IL-9 induction. J Leukoc Biol 2017;101:727–737.
38. Kinnebrew MA, Buffie CG, Diehl GE, et al. Interleukin 23 production by intestinal CD103(+)CD11b(+) dendritic cells in response to bacterial flagellin enhances mucosal innate immune defense. Immunity 2012;36:276–287.
39. Sano T, Huang W, Hall JA, et al. An IL-23R/IL-22 circuit regulates epithelial serum amyloid A to promote local effector Th17 responses. Cell 2015;163:381–393.
40. Zenewicz LA. IL-22: there is a gap in our knowledge. Immunohorizons 2018;2:198–207.
41. Pai YC, Weng LT, Wei SC, et al. Gut microbial transcytosis induced by tumor necrosis factor-like 1A-dependent activation of a myosin light chain kinase splice variant contributes to IBD. J Crohns Colitis 2020;15:258–272.
42. Beumer J, Clevers H. Cell fate specification and differentiation in the adult mammalian intestine. Nat Rev Mol Cell Biol 2021;22:39–53.
43. Gout S, Morin C, Houle F, et al. Death receptor-3, a new E-Selectin counter-receptor that confers migration and survival advantages to colon carcinoma cells by triggering p38 and ERK MAPK activation. Cancer Res 2006;66:9117–9124.
44. Liu C, Li XX, Gao W, et al. Progranulin-derived Atsttrin directly binds to TNFRSF25 (DR3) and inhibits TNF-like ligand 1A (TL1A) activity. PLoS One 2014;9:e92743.
45. Madireddi S, Eun SY, Mehta AK, et al. Regulatory T cell-mediated suppression of inflammation induced by DR3 signaling is dependent on galectin-9. J Immunol 2017;199:2721–2728.
46. Ungaro R, Fukata M, Hsu D, et al. A novel Toll-like receptor 4 antagonist antibody ameliorates inflammation but impairs mucosal healing in murine colitis. Am J Physiol Gastrointest Liver Physiol 2009;296:G1167–G1179.
47. Hamade H, Stamps JT, Stamps DT, et al. BATF3 protects against metabolic syndrome and maintains intestinal epithelial homeostasis. Front Immunol 2022;13:841065.
48. Sato T, Vries RG, Snippert HJ, et al. Single Lgr5 stem cells build crypt-villus structures in vitro without a mesenchymal niche. Nature 2009;459:262–265.
49. Dekkers JF, Alieva M, Wellens LM, et al. High-resolution 3D imaging of fixed and cleared organoids. Nat Protoc 2019;14:1756–1771.


Current address of Y.S.: Department of Gastroenterology and Neurology, Akita University Graduate School of Medicine, Akita City, Japan.

**Received April 11, 2022. Accepted March 28, 2023.**

**Correspondence**
Address correspondence to: Kathrin S. Michelsen, PhD, F. Widjaja Foundation Inflammatory Bowel Disease Institute, Cedars-Sinai Medical Center, Davis Research Building, Room 4012, 110 George Burns Road, Los Angeles, California 90048. e-mail: kathrin.michelsen@cshs.org.

**Acknowledgments**
The authors would like to thank the Cedars-Sinai Medical Center Confocal Microscopy Core, Flow Cytometry Core, and Biobank and Translational Research Core for the support received.

**CRediT Authorship Contributions**

Yosuke Shimodaira (Conceptualization: Lead; Data curation: Lead; Formal analysis: Lead; Investigation: Lead; Methodology: Lead; Project administration: Supporting; Validation: Lead; Visualization: Lead; Writing – original draft: Equal; Writing – review & editing: Equal)

Shyam K. More (Conceptualization: Supporting; Data curation: Supporting; Formal analysis: Supporting; Investigation: Supporting; Methodology: Supporting; Validation: Supporting; Visualization: Supporting; Writing – original draft: Supporting; Writing – review & editing: Supporting)

Hussein Hamade (Conceptualization: Supporting; Data curation: Supporting; Investigation: Supporting; Methodology: Supporting; Writing – review & editing: Supporting)

Anna Y. Blackwood (Data curation: Supporting; Formal analysis: Supporting; Investigation: Supporting; Methodology: Supporting)

Jay P. Abraham (Data curation: Supporting; Formal analysis: Supporting; Investigation: Supporting; Methodology: Supporting)

Lisa S. Thomas (Data curation: Supporting; Formal analysis: Supporting; Investigation: Supporting; Methodology: Supporting)

Jordan H. Miller (Formal analysis: Supporting; Investigation: Supporting; Methodology: Supporting)

Dalton T. Stamps (Formal analysis: Supporting; Investigation: Supporting; Methodology: Supporting)

Sofi L. Castanon (Formal analysis: Supporting; Investigation: Supporting; Methodology: Supporting)

Noam Jacob (Conceptualization: Supporting; Formal analysis: Supporting; Writing – review & editing: Supporting)

Connie W. Y. Ha (Methodology: Supporting; Resources: Supporting) Suzanne Devkota (Methodology: Supporting; Resources: Supporting)

David Q. Shih (Conceptualization: Supporting; Supervision: Supporting)

Stephan R. Targan (Conceptualization: Supporting; Funding acquisition: Lead; Project administration: Supporting; Writing – review & editing: Supporting)

Kathrin S Michelsen (Conceptualization: Lead; Data curation: Supporting; Formal analysis: Supporting; Funding acquisition: Supporting; Project administration: Lead; Supervision: Lead; Validation: Equal; Visualization: Equal; Writing – original draft: Equal; Writing – review & editing: Lead)

**Conflicts of interest**
SRT owns stock in Prometheus Biosciences Inc. and is a consultant for Prometheus Biosciences. The remaining authors disclose no conflicts.

**Funding**
Supported by National Institutes of Health grant DK056328 (S.R.T.), and the F. Widjaja Foundation (S.R.T. and K.S.M.).